Nucleic Acids Research, 2024, **52**, 4295–4312
https://doi.org/10.1093/nar/gkae102
Advance access publication date: 28 February 2024
Gene regulation, Chromatin and Epigenetics

Novel insights into the role of translesion synthesis polymerase in DNA incorporation and bypass of 5-fluorouracil in colorectal cancer

Jameson R. Averill[†], **Jackson C. Lin**[†], **John Jung and Hunmin Jung**[*]

Division of Medicinal Chemistry, School of Pharmacy, University of Connecticut, Storrs, CT 06269, USA

[*]To whom correspondence should be addressed. Tel: +1 860 486 7155; Email: hunmin.jung@uconn.edu
[†]The first and second authors should be regarded as Joint First Authors.

Abstract

5-Fluorouracil (5-FU) is the first-line chemotherapeutic agent in colorectal cancer, and resistance to 5-FU easily emerges. One of the mechanisms of drug action and resistance of 5-FU is through DNA incorporation. Our quantitative reverse-transcription PCR data showed that one of the translesion synthesis (TLS) DNA polymerases, DNA polymerase η (polη), was upregulated within 72 h upon 5-FU administration at 1 and 10 μM, indicating that polη is one of the first responding polymerases, and the only TLS polymerase, upon the 5-FU treatment to incorporate 5-FU into DNA. Our kinetic studies revealed that 5-fluoro-2′-deoxyuridine triphosphate (5FdUTP) was incorporated across dA 41 and 28 times more efficiently than across dG and across inosine, respectively, by polη indicating that the mutagenicity of 5-FU incorporation is higher in the presence of inosine and that DNA lesions could lead to more mutagenic incorporation of 5-FU. Our polη crystal structures complexed with DNA and 5FdUTP revealed that dA:5FdUTP base pair is like dA:dTTP in the active site of polη, while 5FdUTP adopted 4-enol tautomer in the base pairs with dG and HX increasing the insertion efficiency compared to dG:dTTP for the incorrect insertions. These studies confirm that polη engages in the DNA incorporation and bypass of 5-FU.

Graphical abstract

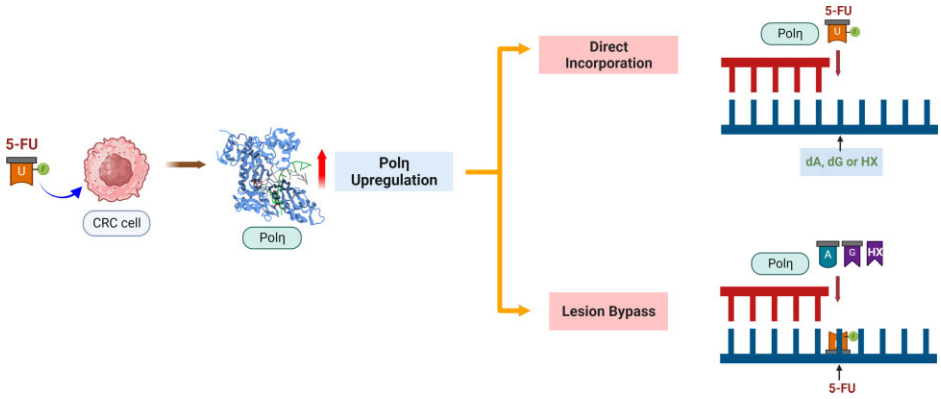

Introduction

Colorectal cancer (CRC) is the third most frequent cancer among all cancers in the world, and low survival and high recurrence rates caused by drug resistance to the current chemotherapeutic regimen along with the facile metastasis are serious problems in CRC (1,2). Despite the recent development of a wide range of cancer therapeutics, the resistance to the approved anti-cancer drugs poses a serious problem in all types of cancers. One of the drugs with a serious resistance problem, especially in CRC, is 5-fluorouracil (5-FU), and 5-FU has long been used as a first-line chemotherapeutic agent for various cancers including CRC. 5-FU has been used to treat CRC with other drugs as combination regimens such as FOLFOX (5-FU, leucovorin and oxaliplatin) along with other regimens including FOLFOX-4, FOLFOX-6 and modified FOLFOX-6 (3–5). In cells, including cancer cells, 5-FU is converted into 5-fluoro-2′-deoxyuridine and then to the monophosphate (5FdUMP) by the series of actions of thymidine phosphorylase (TP) and thymidine kinase (TK) to inhibit thymidylate synthase (TS/TYMS) (6), and 5FdUMP forms a dead-end inhibitor with TYMS (Figure 1A). 5FdUMP/5FUMP can also be further processed to the triphosphate (5FdUTP/5FUTP) form to exert cytotoxicity via direct incorporation into DNA or RNA (7) (Figure 1A). When 5-FU is incorporated into DNA, it can form various base pairs with dA via canonical Watson–Crick base pair (Figure 1B), with

Received: September 10, 2023. **Revised:** January 12, 2024. **Editorial Decision:** January 30, 2024. **Accepted:** February 1, 2024

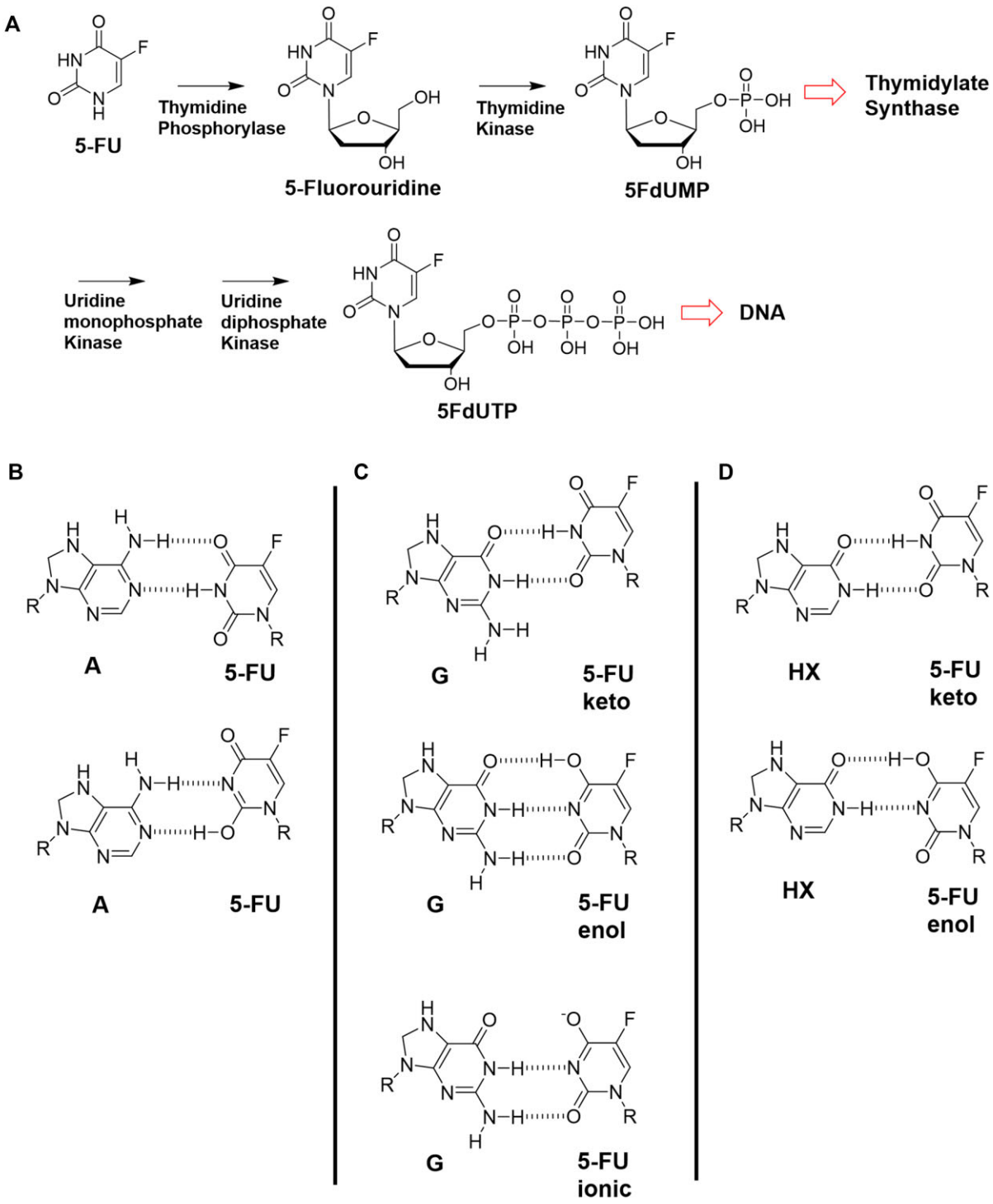

Figure 1. (**A**) 5-fluorouracil (5-FU) can exert its cytotoxic effect via two major pathways. One is by forming a dead-end complex with thymidylate synthase (TYMS) and the other is to incorporate 5-FU into DNA via 5FdUTP. (**B**) Adenine and 5-FU can form a stable Watson–Crick base pair (top), which is favorable, or a wobble base pair (bottom) without engaging any tautomer. (**C**) HX and 5-FU can form a wobble base pair via the keto form of 5-FU (top) or a Watson–Crick like base pair via 4-enol-2-keto tautomer of 5-FU (bottom). (**D**) Guanine and 5-FU can form a wobble base pair via the keto form of 5-FU (top) and a Watson–Crick base pair via 4-enol-2-keto tautomer of 5-FU (bottom).

hypoxanthine (HX) via Watson–Crick like base pair utilizing 4-enol-2-keto tautomer of 5FdUTP (Figure 1C), and with dG via Watson–Crick like base pair utilizing 4-enol-2-keto tautomer of 5FdUTP (Figure 1D). The direct DNA incorporation of 5-FU via 5FdUTP has been confirmed by several research groups in various cells including HeLa, L1210, human neoplastic cells, human breast carcinoma cells and other cancer cells (8–13). The incorporation of 5-FU into RNA or DNA upon the administration of 5-FU in several cancer cells or tissues from cancer patients was shown to happen as early as 24 h according to several studies utilizing gas chromatography-mass spectrometry (GC-MS)-based assays (14–16).

There are several additional mechanisms for CRC cells to acquire resistance to 5-FU, and one of the mechanisms, into which our research here specifically looks, is through translesion synthesis (TLS). There were several reports linking DNA lesion bypass/TLS and cancer drug resistance. One of the drug resistance mechanisms caused by cisplatin was via DNA repair and bypass, and the suppression of Rev1, one of the crucial enzymes in TLS, was found to inhibit the mutagenesis induced by cisplatin and/or cyclophosphamide (17,18). Not just Rev1, DNA polymerase eta (polη) was also reported to be upregulated by several crosslink inducing agents such as mustophoran, mafosfamide or lomustine in breast cancer, glioma and melanoma cells (19). Recently, there also was a report that showed one of the TLS enzymes, Rev7, is closely related to 5-FU and oxaliplatin resistance in CRC (20). The removal of 5-fluorouracil by uracil DNA glycosylase (UDG) superfamily, especially UDG and methyl-CpG binding domain 4 (MBD4), in cancer cells was also reported to be closely related to 5-FU resistance (21,22), though some reports demonstrated little direct relationship between the loss of UDG/MBD4 and 5-FU resistance (23,24). Mutations in MBD4, along with its crucial relationship with mis-match repair (MMR), were reported to exhibit high microsatellite instability (MSI-H) in CRC (25,26).

The deamination of cytosine, adenine and guanine can produce uracil, hypoxanthine (HX) and xanthine (XT), respectively (27,28), and HX, one of the most abundant lesions, was chosen in our study to investigate the relationship between the DNA incorporation of 5-FU and the pre-existing DNA lesions. HX was reported to be efficiently bypassed by human DNA polymerase eta (polη) with high mutagenicity (29), and polη incorporated dCTP opposite HX almost exclusively, recognizing HX the same as guanine. We recently reported that inosine can also be directly incorporated into DNA via deoxyinosine triphosphate (dITP) by polη (30). The mutagenic potential of HX was also displayed in the studies based on human cell lines such as HEK293 and HCT116 as well (31).

The triphosphate forms of canonical and non-canonical nucleotides are removed by inosine triphosphate pyrophosphatase (ITPase), which is encoded by the *ITPA* gene (32), and the genetic defects in *ITPA* gene is closely related to various human diseases such as early infantile encephalopathy (33), infantile dilated cardiomyopathy (34) and neural depolarization and epilepsy (35). Ham1p, a yeast homolog of ITPase, was reported to remove the triphosphate form of non-canonical pyrimidines including 5-FU and the overexpression of Ham1p may contribute to the 5-FU resistance (36,37). T:G mismatch is one of the most frequently occurring mismatches in genomic DNA (38), and it plays a crucial role in the misincorporation of lesions into DNA (30). The formation of T:G mismatch can occur via several ways including via 5-methylcytosine (39) or via spontaneous inserting error by some DNA polymerases including polβ (40) or polλ (41), and T:G mismatch in dsDNA is recognized and repaired by the base excision repair (BER) (42,43).

To study the mutagenic incorporation of 5FdUTP into DNA and the role of TLS DNA polymerases in 5FdUTP incorporation and the drug resistance of 5-FU especially in CRC, we conducted a cell biological investigation on the HCT116 cell line via reverse-transcription real time quantitative PCR (qRT-PCR) to check the upregulation of the genes involved in DNA bypass, DNA repair and nucleotide biosynthesis, all of which are closely related to the incorporation of 5-FU into DNA. Our qRT-PCR studies displayed that one of the Y-family DNA polymerases, human DNA polymerase η (polη), which plays a vital role in one of the DNA lesion bypass processes called translesion synthesis (TLS), was upregulated upon the administration of 5-FU. There are several DNA polymerases, both eukaryotic (44–47) and prokaryotic (48–50), which are utilized in the process of TLS. Polη has been shown to efficiently bypass a wide range of DNA lesions including 8-oxoguanine (8-oxoG), 8-oxoadenine (8-oxoA) (51,52), cisplatin-GG intrastrand cross-link adducts (53), thymine-thymine cyclobutane dimer (54), O6-methylguanine (55), N7-methylguanine (N7mG) (56), N7-benzylguanine (N7BnG) (57), N7-nitrogen half-mustard guanine (NHMG) (58), and hypoxanthine (HX) and xanthine (XT) (29). The contributing factors that affect the mutagenic bypass by polη and other TLS polymerases have been well compiled in several reviews as well (47,59). We also recently showed that polη can incorporate dITP into DNA across dC or dT (30), which indicates that polη might be employed in the first step of introducing any DNA lesion such as inosine or 5-FU into DNA on top of its well-known function of DNA lesion bypass.

Herein, we report the results from qRT-PCR experiments for the regulation of gene expression for the genes that are involved in DNA replication, TLS and nucleotide synthesis in response to the administration of 5-FU from HCT116 colon cancer cell line highlighting the involvement of polη in the incorporation of 5-FU into DNA, along with the kinetic data for 5-FdUTP incorporation opposite the templating dA, dG and HX by human polη. We also report the crystal structures of polη in complex with the incoming 5FdUTP across dA, dG and HX containing DNA in the presence of calcium chloride. These human TLS DNA polymerase-based studies will provide new insights into the role of polη in 5-FU misincorporation via 5FdUTP and the lesion bypass, the mutagenic potential of the incorporation of 5-FU, and their implication in replication, genome instability and TLS. The incorporation and bypass of 5-FU are closely related to the drug action and resistance, and our study presented here will be able to provide novel insights into the mechanism of 5-FU related drug resistance and into the roles of TLS polymerases in 5-FU drug action and resistance.

Materials and methods

Expression and purification of the catalytic domain of polη

Polη catalytic domain (1–432 aa) was expressed and purified using the previously described procedures with slight modifications (54,60). Briefly, polη in pET28a vector was transformed and overexpressed in *Escherichia coli* BL21(DE3)

competent cells, and the cultures in LB media were grown at 37°C until OD_{600} of the culture reached about 0.7. After cooling down the culture to 18°C, the cells were induced with 0.25 mM isopropyl β-D-α-thiogalactopyranoside (IPTG). The induced cells were further grown overnight at 18°C, and the cultured cells were pelleted by centrifugation at 5000 *g* for 30 min. The pelleted cells were collected and kept in −80°C for future use. The frozen pellet was resuspended in Ni column binding buffer A (50 mM sodium phosphate, pH 7.5, 500 mM NaCl and 10% glycerol) that was supplemented with 1 mg/ml lysozyme, 0.25% Nonidet P-40 (NP-40), 0.25% Triton X-100 and 0.25 mM phenylmethylsulfonyl fluoride (PMSF), and the resuspended cells were lysed via sonication for 90 s total (three rounds of 30 s). The lysate was then centrifuged at 16 000 *g* at 4°C for 45 min, and the supernatant was filtered through 0.22 μm syringe filter and loaded onto Ni–NTA column (GE Healthcare) for purification. The eluted fractions were pooled based on the purity checked via SDS-PAGE and further purified using the Heparin HiTrap column (GE Healthcare) followed by Superdex-200 size exclusion chromatography (GE Healthcare). The purity of the final S-200 column elution fractions was confirmed by SDS-PAGE gel, concentrated to 9 mg/ml, and the purified/concentrated protein was flash-frozen in liquid nitrogen and stored at −80°C for future use.

HCT116 cell culture and cell treatment with 5-FU

The human colon cancer cell line, HCT116, was used in this study. HCT116 cells were cultured in McCoy's 5A medium (Gibco, 16600082) supplemented with 10% heat-inactivated fetal bovine serum (Gibco, 10437028), 100 units/ml penicillin and 100 μg/ml streptomycin solution (Gibco, catalog number: 15140122). The cells were grown in a humidified incubator at 37°C with 5% CO_2, and the growth media was replaced every 2–3 days. Cells were seeded into 6-well plates (0.3×10^6 cells per well) in triplicate and treated with 1 and 10 μM 5-fluorouracil along with dimethyl sulfoxide (DMSO) and water as a negative control. Following incubation for 10 min, 1, 6, 24, 48 and 72 h, cells were harvested for RNA extraction. RNA expression was measured using reverse-transcription real time quantitative PCR (qRT-PCR).

Gene expression verification via reverse-transcription real time quantitative PCR (qRT-PCR)

The total RNA was extracted from HCT116 cells using Qiagen's RNeasy Micro Kit (Qiagen, 74004) according to the manufacturer's protocol. RNA concentrations were measured using Nanodrop Spectrophotometer (Thermo Fisher Scientific, Waltham, MA). One microgram of the total RNA was reverse transcribed using iScript Reverse Transcription Supermix (Bio-Rad, 1708841) to prepare cDNA. Samples were prepared with Universal SYBR Green Supermix (Bio-Rad, 1725271), and qRT-PCR was performed using the ABI 7500 Fast Real-time PCR system (Applied Biosystems, Carlsbad, CA). The following thermal protocol was used: 95°C for 2 min for initial denaturation, then 40 cycles of amplification (95°C for 15 s and 60°C for 60 s). RNA levels of the samples were normalized to the housekeeping gene β-actin RNA expression. The fold change in expression was calculated using the 2-ΔΔCT method (triplicates). *P*-values from one-way ANOVA analysis are <0.0001 for all the genes tested except for polκ whose *P*-value is 0.002. The primer sequences are listed below:

Gene Name	Forward	Reverse
β-Actin	GGCACCCAGCACAATGAAG	GCCGATCCACACGGAGTACT
POLK	GTTCTAGTCTCCCAAGCAAGTC	GCTGGCGGTATTCTTGTCTAA
POLH	CATGGAAGGGTGGTGGAATAA	AGCATCATCTGCCCACATAC
POLD	CCAGACCCTCAAGGTACAAAC	CTGCTTGGACTGGAATGAAGA
POLI	GGTGGTTACCTGCAACTATGA	GGGTCAGGTCTTCTCCATTAAC
ITPA	CTTTGTGAGGGTGTCGAGTAG	GTGAATCCTAAGGGCAAGAGAA
POLB	AGCACTAGGGGGTGGAAAGG	CATCATTGGGCCCCCTTTTT
UDG	TTCTAGGAGTCCCTGCTGTGT	TGGTTTGGTCGTGTTGGGTA
MBD4	CGACGTAAAGCCTTTAAGAA	CACATCTCTCCAGTCTGC
TYMS	CCTCGGTGTGCCTTTCAACATC	GGTCTGGGTTCTCGCTGAAGC
POLZ	GAGTTAGGGCCTGGAATATGTG	AGGAGAGGAAGGAGTGAAGAG
REV-1	GTCTCGAACTCCTAACCTTGTG	CCCTTAGAACGTCCACCTTATG

Polη-DNA complex crystallization, data collection, refinement and structure elucidation

To obtain the polη-DNA complex, the undamaged dA/dG containing 12-mer DNA (5′-CAT-[A/G]CTCACACT-3′) and the 8-mer primer (5′-AGTGTGAG-3′) were synthesized by the Integrated DNA Technologies (Coralville, IA), and the HX containing 12-mer DNA (5′-CAT-[HX]CTCACACT-3′) was synthesized by the Keck Oligonucleotide Synthesis facility (Yale School of Medicine, CT). The template and the primer oligonucleotides were annealed in hybridization buffer (10 mM Tris-HCl pH 7.5, 1 mM EDTA) at 90°C for 5 min followed by slow cooling to room temperature. Polη was incubated with the annealed double stranded recessed DNA in a 1:1.5 molar ratio. Subsequently, a 10-fold molar excess of 5FdUTP (Jena Bioscience) was added to the binary complex of polη-DNA in the presence of $CaCl_2$. Ternary polη-DNA (containing dA, dG, or HX):5FdUTP crystals were grown in a buffer solution containing 100 mM 2-(N-morpholino)ethanesulfonic acid (MES) pH 6.5, 14–23% PEG2000 MME and 5 mM $CaCl_2$. The mature crystals were cryoprotected in 20% glycerol supplemented with mother liquor and were flash-frozen in liquid nitrogen. X-ray diffraction data were collected at 100 K at the beamline 17-ID-1 (AMX) and 17-ID-2 (FMX) in National Synchrotron Light Source II (NSLS-II) at Brookhaven National Laboratory. All diffraction data were processed following the data collection onsite using XDS (61,62) and aimless (63,64), and the structures were solved by molecular replacement using Molrep (65) with polη structure with an undamaged DNA (PDB ID 4O3N) as a search model. The model was built in using COOT (66) and refined using PHENIX (67). MolProbity was used to make Ramachandran plots (68). All the crystallographic figures were generated using Chimera (69).

Steady-state kinetics of single nucleotide incorporation of 5FdUTP opposite templating dA/dG/HX by polη

Steady-state kinetic parameters for insertion of 5FdUTP opposite the templating dA/dG/HX by polη were measured as described previously with modification (29). Briefly, the oligonucleotide DNAs for kinetic assays the 13-mer primer, 5′-FAM/GGGGGAAGGATTC-3′, and the 18-mer template, 5′-TCAT(A/G/HX)GAATCCTTCCCCC-3′) were synthesized by the Integrated DNA Technologies (Coralville, IA) and the Keck Oligonucleotide Synthesis facility (Yale School of Medicine, CT). To prepare DNA substrate containing dA, dG

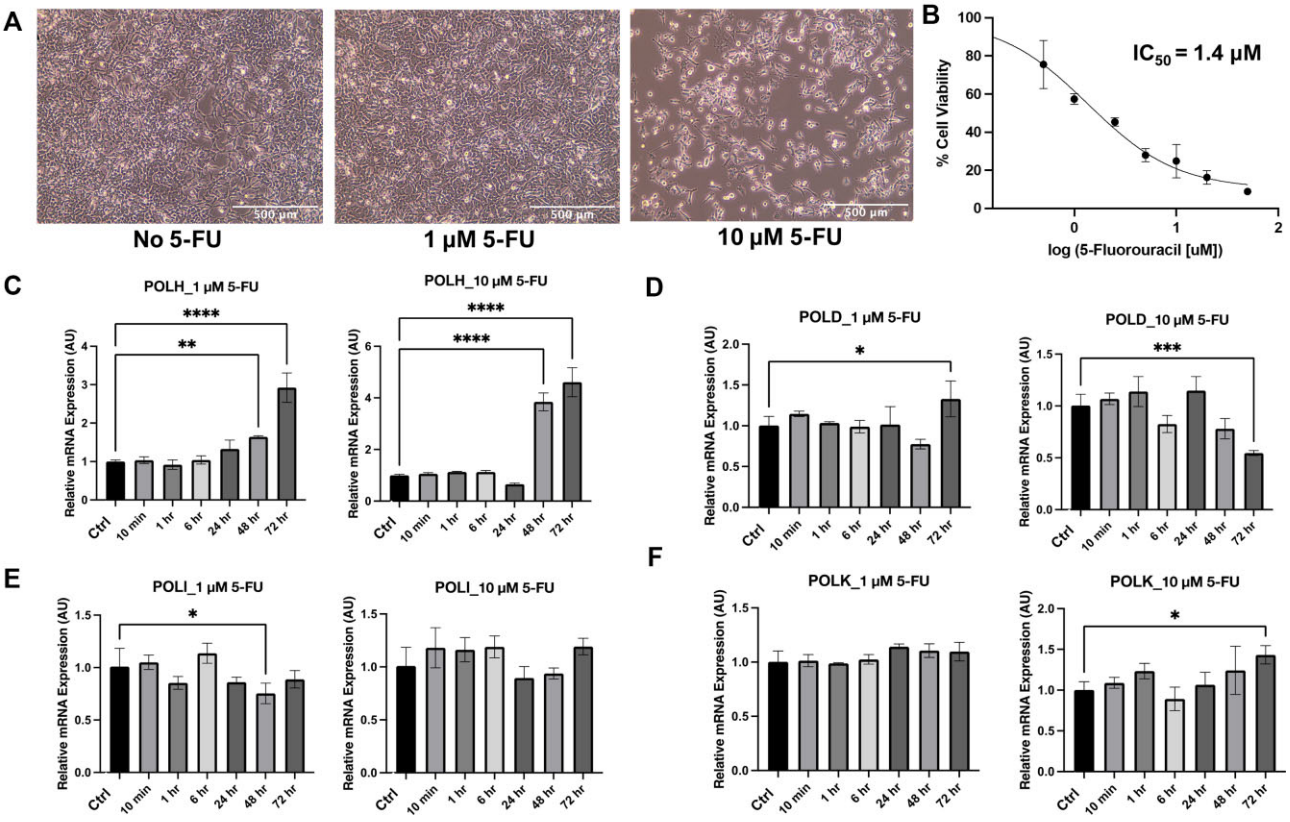

Figure 2. Cell-based assay of 5-FU treatment on HCT116 colon cancer cell line via qRT-PCR. (**A**) HCT116 cells responded sensitively to 5-FU treatment at 1 μM (~40%) and 10 μM (~75%) within 72 h upon the 5-FU treatment. (**B**) IC_{50} of 5-FU on HCT116 cell line based on the cell viability assay was shown to be approximately 1.4 μM. Time-course studies of 5-FU treatment at 1 and 10 μM on HCT116 were analyzed by qRT-PCR for the genes of our interest (**C**) polη, (**D**) polδ, (**E**) polι and (**F**) polκ. *P*-values from one-way ANOVA analysis are <0.0001 for all the genes tested except for polκ whose *P*-value is 0.002.

or HX for the incorporation of 5FdUTP by polη, the template and the primer oligonucleotides were annealed in hybridization buffer (10 mM Tris-HCl pH 7.5, 1 mM EDTA) at 90°C for 5 min followed by slow cooling to room temperature. Enzyme activities were determined using a reaction mixture containing 40 mM Tris-HCl, pH 8.0, 60 mM KCl, 10 mM dithiothreitol, 250 μg/ml bovine serum albumin, 2.5% glycerol, 5 mM $MgCl_2$, 80 nM recessed DNA containing dA, dG or HX, and 8-serial concentrations of incoming 5FdUTP at 37°C. To prevent end-product inhibition and substrate depletion from interfering with the accurate velocity measurement, the enzyme concentrations and reaction-time intervals were adjusted for every experiment (<20% insertion product formed). The reactions were initiated by the addition of the incoming nucleotide (5FdUTP) and stopped with a gel-loading buffer (95% formamide with 20 mM EDTA, 45 mM Tris-borate, 0.1% bromophenol blue, 0.1% xylene cyanol). The quenched samples were separated on 18% denaturing urea-polyacrylamide gels. The gels were analyzed using ChemiDoc MP and Image Lab Software (BioRad) to quantify product formation. The k_{cat} and K_m values were determined by fitting reaction rate over 5FdUTP concentrations to Michaelis–Menten and Lineweaver–Burk equations. Each experiment was repeated three times to measure the average of the kinetic parameters along with the standard deviation. The efficiency of nucleotide insertion was calculated as k_{cat}/K_m, and the relative frequency of 5FdUTP incorporation opposite dG/HX over dA was determined as $f = (k_{cat}/K_m)_{[dG/HX:5FdUTP]} / (k_{cat}/K_m)_{[dA:5FdUTP]}$.

Results

Polη was upregulated upon 5-FU treatment in HCT116cell line

To evaluate whether the administration of 5-FU and its misincorporation into DNA affects the regulation of gene expression in HCT116, a colon cancer cell line, we performed the reverse-transcription real time quantitative polymerase chain reaction (qRT-PCR) with mRNA samples extracted from HCT116 cells treated with 5-FU. For the time-course experiments, the samples were taken in 10 min, 1, 6, 24, 48 and 72 h after the treatment of 5-FU for the mRNA extraction and qRT-PCR experiments. The 72-h treatment of 1 μM 5-FU killed approximately 40% of HCT116 cells and 10 μM 5-FU treatment killed approximately 75% of HCT116 cells (Figure 2A), and the IC_{50} of 5-FU on HCT116 cells was found to be 1.4 μM (Figure 2B). According to the qRT-PCR experiments with the mRNA extracted from HCT116 cells, polη, which is one of the main DNA polymerases employed in TLS, was upregulated at both 1 and 10 μM 5-FU (Figure 2C). At 1 μM 5-FU, polη was upregulated about 3-fold in 72 h, while it was upregulated about 4-fold in 48 h at 10 μM 5-FU (Figure 2C).

Other TLS polymerases, polι or polκ, were not significantly upregulated upon 5-FU treatment in HCT116 cell line

One of the replicative DNA polymerases, polδ, was not significantly upregulated by the administration of 5-FU at either 1 or 10 μM (Figure 2D). This is a quite intriguing finding, in

Table 1. Kinetic parameters for 5FdUTP incorporation opposite dA, dG, and HX by polη

Template:dNTP	K_m (μM)	k_{cat} (10^{-3} s^{-1})	k_{cat}/K_m (10^{-3} s^{-1} μM^{-1})	f^a
polη				
dA:5FdUTP	8.3 ± 0.6	84.7 ± 4.2	10.3	1
dG:5FdUTP	105.9 ± 13.4	26.7 ± 1.4	0.25	0.024
HX:5FdUTP	69.9 ± 4.6	25.9 ± 0.4	0.37	0.036
dA:dTTP	6.5 ± 0.4	89.2 ± 2.9	13.6	1
dG:dTTP	130.9 ± 9.5	21.4 ± 3.0	0.16	0.012
HX:dTTP	111.7 ± 3.7	17.2 ± 2.0	0.15	0.011
dA:dUTP	7.1 ± 0.4	87.3 ± 3.1	12.4	1
dG:dUTP	124.7 ± 8.5	22.9 ± 4.5	0.18	0.014
HX:dUTP	121.6 ± 5.8	21.3 ± 4.6	0.17	0.013
dA:dCTP	90.2 ± 5.6	10.9 ± 1.2	0.12	0.007
dG:dCTP	4.8 ± 0.5	81.6 ± 5.8	17.0	1
HX:dCTP	6.2 ± 0.8	75.0 ± 6.4	12.1	0.71
HX:dCTP (polκ)[b]	1.36 ± 0.4	171.7 ± 7.3	126.3	1
HX:dTTP (polκ)[b]	23.5 ± 6.9	25.0 ± 1.8	1.06	0.008
HX:dCTP (polα)[b]	0.73 ± 0.26	7.8 ± 0.5	10.7	1
HX:dTTP (polα)[b]	9.74 ± 1.6	1.83 ± 1.17	0.19	0.018

[a]Relative efficiency:$(k_{cat}/K_m)_{[dTTP:dT]}/(k_{cat}/K_m)_{[dTTP:dC]}$ or $(k_{cat}/K_m)_{[dGTP:dT]}/(k_{cat}/K_m)_{[dGTP:dC]}$
[b]Reference (70)

that it might indicate that polη, not a replicative DNA polymerase, is used first to incorporate 5-FU into DNA. Another intriguing finding was that other TLS polymerases, DNA polymerase iota (polι) and kappa (polκ), were not significantly upregulated upon the administration of 5-FU at either 1 or 10 μM (Figure 2E and F). In HCT116 cells at least, polη was the only TLS polymerase that was upregulated in response to the treatment of 5-FU, and this might be a specific response closely related to the 5-FU resistance in HCT116 cell line and colorectal cancer or a broad-spectrum effect that can be applied to a wide range of cancer cells.

Incorporation of 5FdUTP across undamaged dA by polη is highly efficient

To evaluate whether the incorporation of 5FdUTP across undamaged and damaged template bases by polη is promutagenic, we determined the kinetic parameters for polη incorporating 5FdUTP opposite templating dA and dG along with the control incorporation of 5FdUTP across one of DNA lesions, HX (Table 1 and Figure 3). Polη inserted 5FdUTP opposite dA, which is a favorable incorporation, with catalytic efficiency of 10.3 in terms of k_{cat}/K_m and the relative efficiency of 0.76 compared with the control incorporation of dTTP opposite dA (13.6 for dA:dTTP versus 10.3 for dA:5FdUTP), indicating that polη quite readily incorporated 5FdUTP across dA with just slightly less efficiency compared to a canonical incorporation of dTTP across dA. The turnover numbers (k_{cat}) for both incorporations, dA:dTTP and dA:5FdUTP, were similar (89.2 s^{-1} versus 84.7 s^{-1}), but the K_m value was slightly higher in dA:5FdUTP (6.5 μM versus 8.3 μM). This indicates that 5FdUTP incorporation needs a slightly higher concentration of the incoming nucleotide, 5FdUTP, than the correct insertion of dA:dTTP. Still, the reaction is as facile as dTTP incorporation once enough 5FdUTP is bound in the active site of polη. A more detailed insight will be given with the crystal structures in the later sections.

Polη Incorporated 5FdUTP across dG more efficiently than dTTP incorporation

To evaluate whether the misincorporation of 5FdUTP across the undamaged dG by polη is efficient, we also determined the kinetic parameters for polη incorporating 5FdUTP opposite templating dG along with the control incorporation of dTTP and dCTP across dG (Table 1 and Figure 2). Polη inserted 5FdUTP opposite dG with a catalytic efficiency of 0.25 in terms of k_{cat}/K_m, and the relative efficiency compared to dA:5FdUTP incorporation is 0.024 (10.3 for dA:5FdUTP versus 0.25 for dG:5FdUTP). This catalytic efficiency of 5FdUTP insertion across dG by polη is about 1.5-fold higher than that of dTTP insertion across dG (0.25 versus 0.16), highlighting that polη-mediated incorporation of 5FdUTP is slightly more mutagenic. This mutagenicity becomes even more significant when there is inosine in DNA as will be discussed in the next section. The turnover numbers (k_{cat}) for dG:5FdUTP were about 3.2 times lower than dA:5FdUTP (26.7 s^{-1} versus 84.7 s^{-1}), while the K_m value for dG:5FdUTP was about 13 times higher than that of dA:5FdUTP (105.9 μM versus 8.3 μM). This indicates that 5FdUTP misincorporation across dG needs significantly higher (∼13-fold) nucleotide concentration than the correct incorporation of 5FdUTP opposite dA, but 5FdUTP incorporation across dG has just three times lower turnover rate in the active site of polη than the incorporation of 5FdGTP across dA once enough 5FdUTP is bound. The relative ratio of the catalytic efficiency between correct and incorrect insertion of dTTP (dA vs. dG) by polη is approximately 85:1, while the same ratio for 5FdUTP incorporation is approximately 40:1 indicating that 5FdUTP incorporation has >2-fold higher mutagenicity compared to the canonical incorporations of dTTP (Table 1).

Incorporation of 5FdUTP across inosine (HX) by polη is more efficient than opposite dG

To evaluate whether a pre-existing DNA lesion, such as inosine, can affect the efficiency and mutagenicity of the incorporation of 5FdUTP, we determined the kinetic parameters for polη incorporating 5FdUTP opposite templating HX (Table 1 and Figure 2). Because inosine is formed from adenine via deamination, dTTP insertion across dA can also be considered as control for 5FdUTP incorporation in addition to dTTP/dCTP insertions across dG (Table 1). Polη inserted 5FdUTP opposite HX, which behaves like dG in DNA, with catalytic efficiency of 0.37 in terms of k_{cat}/K_m and the rel-

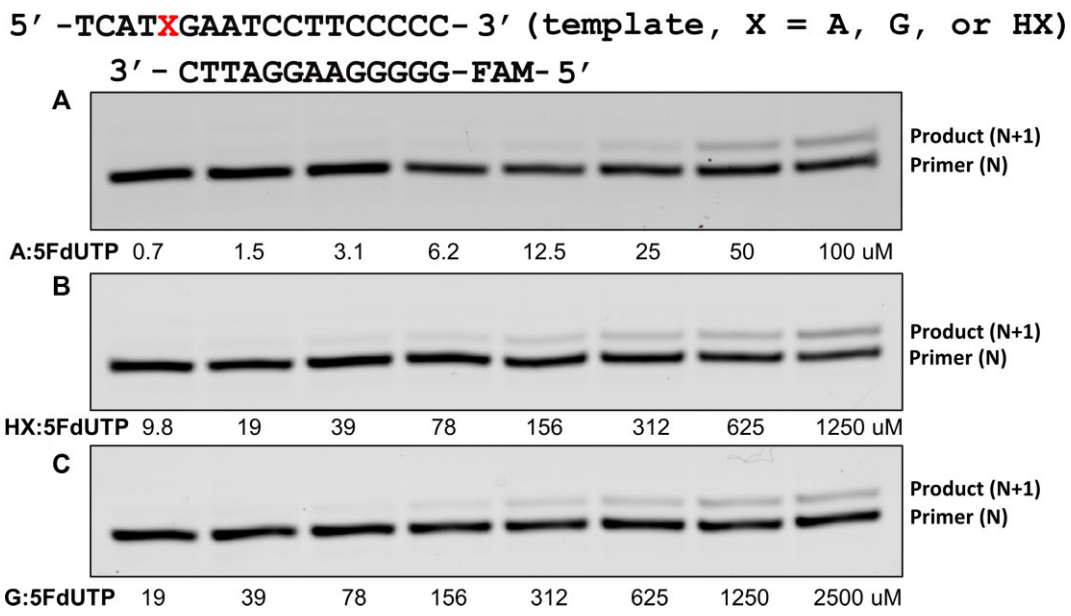

Figure 3. 5-Fluorodeoxyuridine triphosphate (5FdUTP) incorporation opposite templating dA (**A**), HX (**B**) and dG (**C**) by polη. Primer-template dsDNA (18-mer template) was mixed with polη, and the reactions were initiated by addition of eight different concentrations of 5FdUTP. 5′-FAM-labeled primer was used for the single-nucleotide incorporation study, and the reaction was conducted for 1 (dA:5FdUTP) or 2 (dG/HX:5FdUTP) min at 37°C, and the quenched samples were separated on 18% denaturing polyacrylamide gels.

ative efficiency of 0.036 compared to dA:5FdUTP (10.3 for dA:5FdUTP versus 0.37 for HX:5FdUTP). On the other hand, polη inserted 5FdUTP opposite HX with the relative efficiency of 1.48 compared to dG:5FdUTP (0.25 for dG:5FdUTP versus 0.37 for HX:5FdUTP) indicating that polη quite readily incorporated 5FdUTP across HX with slightly higher efficiency compared to the incorporation of 5FdUTP across dG (Table 1). The turnover numbers (k_{cat}) for HX:5FdUTP and dG:5FdUTP were quite similar (25.9 s^{-1} versus 26.7 s^{-1}), while the K_m value for HX:5FdUTP was lower than that of dG:5FdUTP (69.9 μM versus 105.9 μM). This indicates that 5FdUTP incorporation is more efficient compared to opposite dG when there is inosine present in the template DNA, and the required concentration of 5FdUTP is lower when bypassing inosine. Furthermore, the presence of inosine, which works the same as dG in DNA, makes the incorporation of 5FdUTP more mutagenic combined with 5FdUTP insertion opposite dG. When there is no HX, the mutagenic ratio of 5FdUTP incorporation is 40:1 across dA and dG. When HX is present, however, this ratio becomes 16:1 across dA and across dG/HX. From the previously published studies, polα incorporated dCTP and dTTP across HX with a ratio of approximately 60:1, and the ratio was 70:1 in polη and 120:1 in polκ (Table 1) (29,70). In our experiments, polη was shown to incorporate dCTP and dTTP opposite HX with a ratio of about 80:1, while the same ratio for the incorporation of 5FdUTP (dCTP vs. 5FdUTP) is about 30:1 resulting in a higher mutagenicity (Table 1). Overall, these results highlight the effect of HX on the efficiency and mutagenicity of 5FdUTP incorporation by polη.

5FdUTP formed Watson-Crick base pair with the templating dA in the active site of polη

Our kinetic studies showed that polη efficiently incorporated 5FdUTP opposite the templating dA (Table 1), like the canonical incorporation of dTTP across dA. To acquire insights on the structural features of 5FdUTP incorporation into DNA by polη, we elucidated a crystal structure of polη complexed with a recessed dsDNA containing dA with the incoming 5FdUTP in the presence of the divalent calcium ion (Ca^{2+}). Ca^{2+} was reported to inhibit or significantly reduce the primer terminus 3-OH's nucleophilic attack on the alpha phosphate (P_α) of the incoming nucleotide in a lot of DNA polymerases (71,72), and some of the earlier polη structures used Ca^{2+} ion to elucidate pre-insertion structures (73,74). The polη-dA:5FdUTP ternary complex was crystallized in $P6_1$ space group with the cell dimension of a = 97.91 Å, b = 97.91 Å, c = 81.01 Å, α = 90.00°, β = 90.00° and γ = 120.00°. The polη-dA:5FdUTP ternary structure was refined to a resolution of 2.78 Å with R_{work} = 20.5% and R_{free} = 27.9% (Table 2).

The polη-dA:5FdUTP ternary complex structure provides a structural insight on the insertion of 5FdUTP opposite dA by polη (Figure 4), and this crystal structure exhibits the characteristic secondary structures of polη along with the four well-conserved domains of Y-family DNA polymerases, thumb, palm, finger and little finger (Figure 4A). The dA:5FdUTP base pair is well ordered and snugly accommodated in the active site of polη as displayed by the strong and well-defined electron density ($2F_o$-F_c = 1σ) around dA and the incoming 5FdUTP (Figure 4B). 3′-OH of the primer terminus is coordinated with one of the calcium ions and is approxiamtely 3.0 Å away from the Pα of 5FdUTP being optimally poised for in-line nucleophilic attack on the Pα of the 5FdUTP (Figure 4C). The templating dA displayed Watson–Crick geometry in base pairing with the incoming 5FdUTP, and the inter-base hydrogen bonding distances are 2.6 Å (N6 of dA and O4 of 5FdUTP) and 2.5 Å (N1 of dA and N3 of 5FdUTP) between them (Figure 4D). 5-F group of 5FdUTP has a hydrogen bonding interaction with the alpha phosphate group of 5FdUTP with the distance of 3.2 Å (Figure 4D), which works as an anchor for the uracil ring in the active site of polη. The geometry of dA:5FdUTP base pair displayed the λ angles of 50.5°

Table 2. Data Collection and Refinement Statistics

PDB CODE	Polη dA:5FdUTP (8GKR)	Polη HX:5FdUTP (8SKI)	Polη dG:5FdUTP (8GML)
Data Collection			
space group	$P6_1$	$P6_1$	$P6_1$
(a) Cell Constants			
a (Å)	97.907 97.907	98.560 98.560	98.822 98.822
B	81.008	81.094	81.184
c	90.00	90.00	90.00
α (°)	90.00	90.00	90.00
β	120.00	120.00	120.00
γ			
Resolution (Å)[a]	58.57–2.78 (2.84–2.78)	58.79–2.16 (2.20–2.16)	58.90–2.57 (2.62–2.57)
R_{merge}[b] (%)	0.092 (0.737)	0.058 (0.711)	0.098 (0.736)
<I/σ>	7.8 (1.3)	9.9 (1.2)	7.3 (1.2)
$CC_{1/2}$ (Highest resolution)	0.484	0.482	0.436
Completeness (%)	93.3 (100.0)	100.0 (100.0)	100.0 (100.0)
Redundancy	13.2 (13.4)	13.5 (13.3)	13.4 (13.6)
Refinement			
R_{work}[c]/R_{free}[d] (%)	20.5/27.9	20.2/24.9	20.4/26.0
Unique reflections	10363	23984	14501
Mean B Factor (Å^2)			
Protein	53.38	41.98	49.83
Ligand	58.12	48.11	54.86
Solvent	50.26	41.70	44.16
Ramachandran Plot			
Most favored (%)	92.7	97.7	96.0
Add. allowed (%)	6.7	2.1	3.6
RMSD			
Bond lengths (Å)	0.010	0.009	0.010
Bond angles (degree)	1.140	1.105	1.174

[a]Values in parentheses are for the highest resolution shell.
[b]$R_{merge} = \Sigma|I-\langle I\rangle| / \Sigma I$ where I is the integrated intensity of a given reflection.
[c]$R_{work} = \Sigma||F(obs)|-|F(calc)||/\Sigma|F(obs)|$.
[d]$R_{free} = \Sigma||F(obs)|-|F(calc)||/\Sigma|F(obs)|$, calculated using 5% of the data.

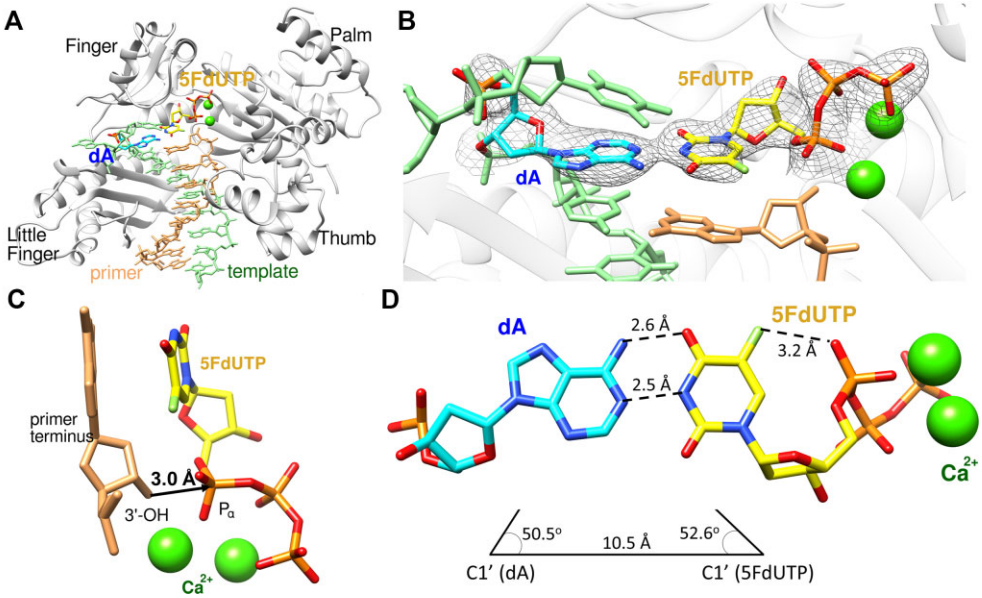

Figure 4. The ternary structure of polη complexed with a recessed dsDNA with templating dA and the incoming 5FdUTP. (**A**) Overall structure of polη complexed with templating dA and the incoming 5FdUTP in the presence of Ca^{2+}. All four subdomains, finger, little finger, thumb and palm, are well conserved. (**B**) The close-up view of the polη-dA:5FdUTP ternary structure. The $2F_o$-F_c electron density around dA and 5FdUTP contoured at 1 σ is shown, and the electron density is well ordered around both dA and 5FdUTP in the active site of polη. (**C**) The incoming nucleotide (5FdUTP) and the metal binding site of polη-dA:5FdUTP display that 3′-OH of the primer is 3.0 Å away from P_α of 5FdUTP with two Ca^{2+} ions well positioned in the active site as well. (**D**) The Watson–Crick base pair between the templating dA and 5FdUTP is shown, and the geometry of the base pair is close to the optimal Watson–Crick base pair.

(dA) and 52.6° (5FdUTP) and the C1′-C1′ distance of 10.5 Å (Figure 4D), which is similar with the geometry of the canonical base pairs.

5FdUTP formed a distorted Watson–Crick like base pair with the templating dG via 4-enol tautomer of 5FdUTP

Our kinetic studies showed that polη less efficiently incorporated 5FdUTP opposite the templating dG compared to the templating dA, yet 5FdUTP incorporation across dG, which would cause G:C to A:T mutation as a result, was slightly more efficient than the incorporation of dTTP opposite dG (0.25 versus 0.16 in k_{cat}/K_m) (Table 1). To gain insights on the structural features of 5FdUTP incorporation opposite dG by polη, we solved another crystal structure of polη complexed with recessed dsDNA containing dG with the incoming 5FdUTP in the presence of calcium chloride. The polη-dG:5FdUTP ternary complex was crystallized in $P6_1$ space group with the cell dimension of $a = 98.82$ Å, $b = 98.82$ Å, $c = 81.18$ Å, $\alpha = 90.00°$, $\beta = 90.00°$ and $\gamma = 120.00°$. The polη-dG:5FdUTP ternary structure was refined to a resolution of 2.57 Å with $R_{work} = 20.4\%$ and $R_{free} = 26.0\%$ (Table 2).

The polη-dG:5FdUTP ternary complex structure provides the structural basis for the incorrect incorporation of 5FdUTP opposite dG by polη (Figure 5). This structure, like polη-dA:5FdUTP, displays the conserved secondary structures and the four characteristic domains (thumb, palm, finger and little finger) of Y-family DNA polymerases (Figure 5A). The dG:5FdUTP base pair is well ordered and accommodated in the catalytic active site of polη as indicated by the well-defined electron density ($2F_o$-$F_c = 1\sigma$) around dG and the incoming 5FdUTP, though the density around the uracil ring is not perfect (Figure 5B). However, the unfavorable base pair between dG and 5FdUTP showed just one catalytic metal in the active site with one calcium missing from the site which is close to 3′-OH of the primer terminus and the primer terminus 3′-OH has no coordination with a calcium ion due to the missing calcium ion. The distance between the primer terminus and the Pα of 5FdUTP is approxiamtely 3.6 Å (Figure 5C) being less than optimally positioned for in-line nucleophilic attack on the Pα of the 5FdUTP. The templating dG formed a Watson–Crick like pair with 5FdUTP via 4-enol tautomer with the inter-base hydrogen bonding distances of 3.2 Å (O6 of dG and O4 of 5FdUTP), 2.8 Å (N1 of dG and N3 of 5FdUTP) and 2.5 Å (N2 of dG and O2 of 5FdUTP) (Figure 5D). 5-FU is known to have a high propensity for 4-enol tautomer, and it was shown that a significant amount of the 4-enol tautomer of 5-FU present in physiological condition (75). 5-FU was also reported to form ionic tautomer, on top of keto and enol forms, and this ionic form can increase the mutagenic incorporation of 5-FU across dG (76,77). However, our crystal structure of polη-dG:5FdUTP indicated that this ionic form may not be utilized in 5FdUTP incorporation by polη. The kinetic data also showed that 5FdUTP incorporation across dG was not as efficient compared to the correct incorporation of 5FdUTP across dA (10.3 for dA:5FdUTP vs. 0.25 for dG:5FdUTP in terms of k_{cat}/K_m). 5-F group of 5FdUTP has a hydrogen bonding interaction with the alpha phosphate group of 5FdUTP with the distance of 3.3 Å (Figure 5D), and this extra interaction might cause the ring distortion between dG and 5FdUTP. The geometry of dG:5FdUTP base pair displayed the λ angles of 59.7° (dG) and 61.6° (5FdUTP) and the C1′-C1′ distance of 9.7 Å (Figure 5D), which is not significantly different from that of correct undamaged base pairs. However, the C1′-C1′ distance is quite short due to the distortion of the purine-pyrimidine rings of dG and 5FdUTP instead of being on the same plane with the angle between the planes of the two rings being 35.7° (Figure 5E), and this propeller distortion makes the interaction between the two rings weaker resulting in the less-than-optimal efficiency of the nucleotide incorporation.

5FdUTP was incorporated across HX forming Watson–Crick like base pair via 4-enol tautomer of 5FdUTP

Our kinetic studies showed that polη less efficiently incorporated 5FdUTP opposite the templating HX compared to the templating dA, and it was approximately 2.5 times more efficient than the incorporation of dTTP opposite HX by polη (0.37 versus 0.15 in k_{cat}/K_m) (Table 1). To gain insights on the structural features of 5FdUTP incorporation opposite HX by polη, we solved another crystal structure of polη complexed with recessed dsDNA containing HX with the incoming 5FdUTP in the presence of calcium chloride. The polη-HX:5FdUTP ternary complex was crystallized in $P6_1$ space group with the cell dimension of $a = 98.56$ Å, $b = 98.56$ Å, $c = 81.09$ Å, $\alpha = 90.00°$, $\beta = 90.00°$ and $\gamma = 120.00°$. The polη-HX:5FdUTP ternary structure was refined to a resolution of 2.16 Å with $R_{work} = 20.2\%$ and $R_{free} = 24.9\%$ (Table 2).

The polη-HX:5FdUTP ternary complex structure provides the structural basis for the incorporation of 5FdUTP opposite HX by polη (Figure 6). This structure, just like polη-dG:5FdUTP, displays the conserved secondary structures and the four characteristic domains (thumb, palm, finger and little finger) of Y-family DNA polymerases (Figure 6A). The HX:5FdUTP base pair is well ordered and snugly accommodated in the catalytic active site of polη as indicated by the well-defined electron density ($2F_o$-$F_c = 1\sigma$) around HX and the incoming 5FdUTP (Figure 6B). However, the base pair between HX and 5FdUTP displayed just one calcium metal in the active site, and the primer terminus 3′-OH has no coordination with a metal due to the missing A-site calcium ion and displayed approximately 3.5 Å distance from the Pα of 5FdUTP (Figure 6C) being less than optimally positioned for in-line nucleophilic attack on the Pα of the 5FdUTP. The templating HX formed a wobble base pair with 5FdUTP with the inter-base hydrogen bonding distances of 3.1 Å between O6 of HX and O4 of 5FdUTP and 2.6 Å between N1 of HX and N3 of the 4-enol tautomer of 5FdUTP (Figure 6D). 5-F group of 5FdUTP has a hydrogen bonding interaction with the α phosphate group of 5FdUTP with the distance of 3.5 Å (Figure 6D), and this extra interaction causes the ring distortion between HX and 5FdUTP just like in dG:5FdUTP. The geometry of HX:5FdUTP base pair displayed the λ angles of 67.1° (HX) and 52.3° (5FdUTP) and the C1′-C1′ distance of 10.2 Å (Figure 6D), which is not significantly different from that of correct undamaged base pairs. However, the C1′-C1′ distance is a little bit shorter than canonical base pairs due to the distortion of the purine-pyrimidine rings of HX and 5FdUTP instead of being on the same plane similar to the base pair between dG:5FdUTP, and the distortion angle between the

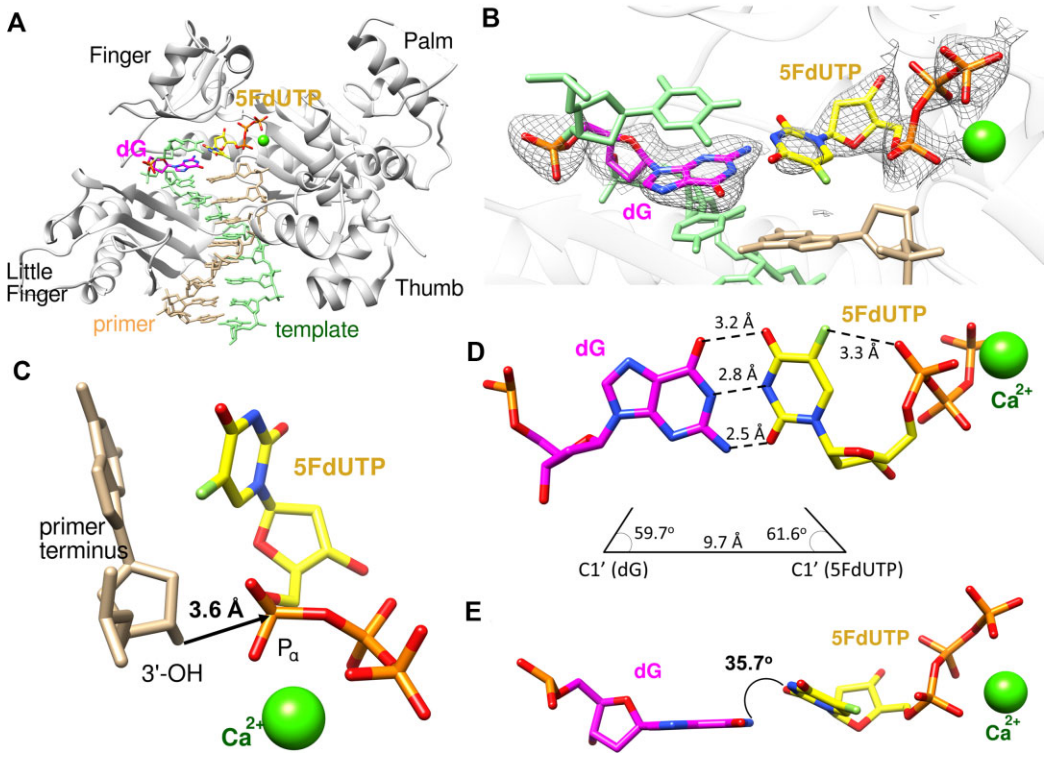

Figure 5. The ternary complex structure of polη complexed with a recessed dsDNA with templating dG and the incoming 5FdUTP. (**A**) Overall structure of polη complexed with templating dG and the incoming 5FdUTP in the presence of Ca^{2+} with all four subdomains, finger, little finger, thumb and palm, are all shown. (**B**) Close-up view of the active site of the polη-dG:5FdUTP ternary structure. The $2F_o$-F_c electron density around dG and 5FdUTP contoured at 1 σ is shown in the active site of polη. (**C**) The incoming nucleotide and metal binding site of polη-dG:5FdUTP displays that 3′-OH of the primer is 3.6 Å away from P_α of 5FdUTP with just one Ca^{2+} ion in the active site. 3′-OH is in an adequate direction and distance for the nucleophilic attack on P_α. (**D**) The Watson–Crick like base pair between dG and 5FdUTP via tautomerization, and 5FdUTP adopted 4-enol tautomer for the base pair with dG. (**E**) Though dG and 5FdUTP formed Watson-Crick like base pair, the distortion between the two rings of the bases is about 36° making the base pair less efficient.

planes of the two rings is 18.7°, which is much smaller than in dG:5FdUTP leading to a higher efficiency for 5FdUTP incorporation (Figure 6E). This difference in the distortion angle might come from the different interactions in the base pairs, two hydrogen bonding interactions in HX:5FdUTP and three in dG:5FdUTP, and more constraint is on dG:5FdUTP base pair in the active site of polη.

5FdUTP incorporation across dA by polη is as efficient as dTTP incorporation

When polη-dA:5FdUTP and polη-dA:dTTP* (PDB ID: 6PL7) structures were superposed, we were able to gain insights into the DNA incorporation of 5FdUTP across dA, which is a correct insertion, by polη. As stated in the previous section, our kinetic studies showed that 5FdUTP incorporation across dA was as efficient as dTTP incorporation across dA (13.6 for dA:dTTP versus 10.3 for dA:5FdUTP in terms of $k_{cat}/K_{m,}$ Table 1). When we superimposed the two crystal structures, they overlapped quite well with the RMSD of 0.36 Å over 424 α-carbons along with similar base pairs in the active site of polη (Figure 7A). Though there is a slightly different position in dA rings (∼0.9 Å) in the two structures, the positions of 5FdUTP and dTTP, along with the positions of the catalytic metals of Ca^{2+} in polη-dA:5FdUTP and Mg^{2+} polη-dA:dTTP* in the same site, overlap well in the active site of polη (Figure 7B). In both base pairs (dA:5FdUTP and dA:dTTP), there was no distortion between the two rings involved leading the incorporation of 5FdUTP across dA as efficient as the canonical incorporation of dTTP across dA.

Less efficient incorporation of 5FdUTP across dG by polη compared to across dA

When polη-dA:5FdUTP and polη-dG:5FdUTP structures were superposed, we were able to gain some insights into the DNA incorporation of 5FdUTP across dG, which is an incorrect insertion, by polη. As presented in the earlier section, our kinetic study showed that 5FdUTP incorporation across dG was approximately 40-fold less efficient than 5FdUTP incorporation across dA (0.25 for dG:5FdUTP versus 10.3 for dA:5FdUTP in terms of $k_{cat}/K_{m,}$ Table 1). When we superimposed the two crystal structures, they overlapped quite well with the RMSD of 0.26 Å over 424 α-carbons (Figure 7C). However, the two base pairs of dG:5FdUTP and dA:5FdUTP showed significant difference in the active site of polη. Approximately 35° distortion of the rings in the base pair between dG and 5FdUTP is clearly seen in the overlapped structures (Figure 7C), and this distortion caused approximately 1.0 Å difference in the positions of 5-fluorouracil rings in the two structures (Figure 7D). Also, one of the catalytic metals missing in the usual position close to Pα of the incoming nucleotide, and the remaining catalytic metal (Ca^{2+}) in the dG:5FdUTP structure lies in a different position than in dA:5FdUTP structure (Figure 7C and D) making the 5FdUTP incorporation across dG less efficient.

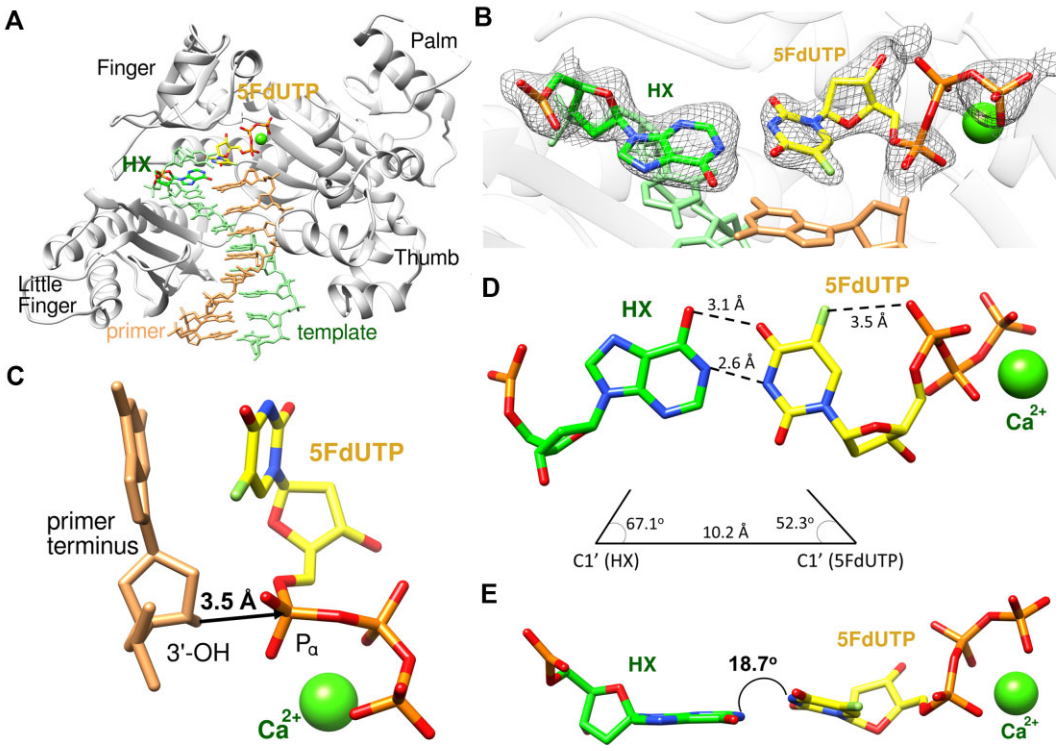

Figure 6. The ternary complex structure of polη complexed with a recessed dsDNA with templating HX and the incoming 5FdUTP. (**A**) Overall structure of polη complexed with templating HX and the incoming 5FdUTP in the presence of Ca^{2+} with all four subdomains, finger, little finger, thumb and palm, are all shown. (**B**) Close-up view of the active site of the polη-HX:5FdUTP ternary structure. The $2F_o$-F_c electron density around HX and 5FdUTP contoured at 1 σ is shown in the active site of polη. (**C**) The incoming nucleotide and metal binding site of polη-HX:5FdUTP displays that 3′-OH of the primer is 3.5 Å away from P_α of 5FdUTP with just one Ca^{2+} ion in the active site. 3′-OH is in a fine direction and distance for the nucleophilic attack on P_α. (**D**) The Watson–Crick like base pair between HX and 5FdUTP via tautomerization. 5FdUTP adopted 4-enol tautomer for the base pair with HX. (**E**) Similar with dG:5FdUTP, HX and 5FdUTP formed Watson–Crick like base pair with the distortion between the two rings of the bases being about 18° making the base pair more efficient than dG:5FdUTP.

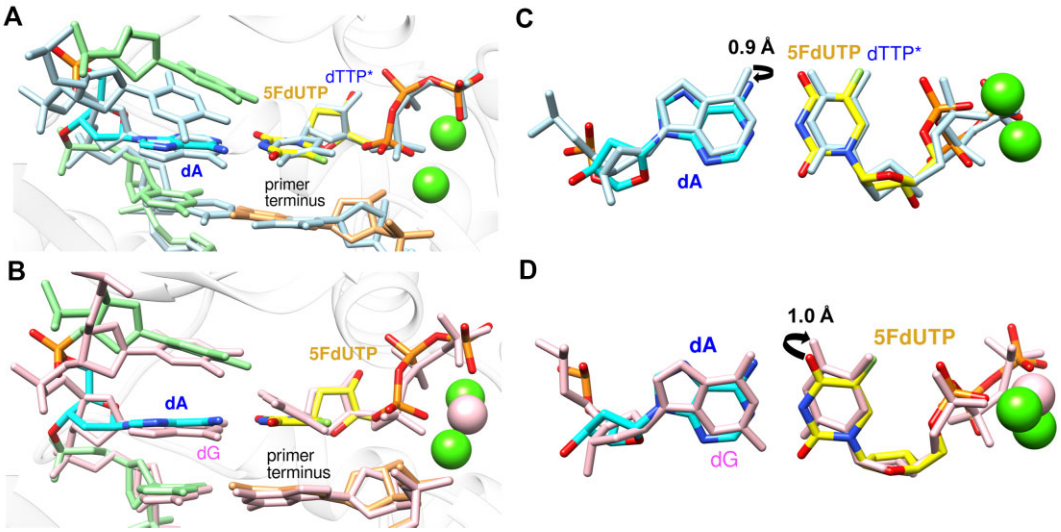

Figure 7. The comparison of the crystal structure of polη-dA:5FdUTP with polη-dA:dTTP* (PDB ID: 6PL7) and polη-dG:5FdUTP. (**A**) Close-up view of the overlapped structures of dA:5FdUTP and dA:dTTP* in the active site of polη. Both base pairs are well ordered and well aligned in the active site. (**B**) The overlapped structures of the base pairs showed that there was slight difference (0.9 Å) in the position of dA in the two structures. (**C**) Close-up view of the overlapped structures of dA:5FdUTP and dG:5FdUTP in the active site of polη. Both base pairs are well ordered and well aligned in the active site. However, dG:5FdUTP base pair displays clear ring distortion compared to dA:5FdUTP with just one calcium ion found in dG:5FdUTP. (**D**) The overlapped structures of the base pairs showed that there was difference (1.0 Å) in the position of 5FdUTP in the two structures.

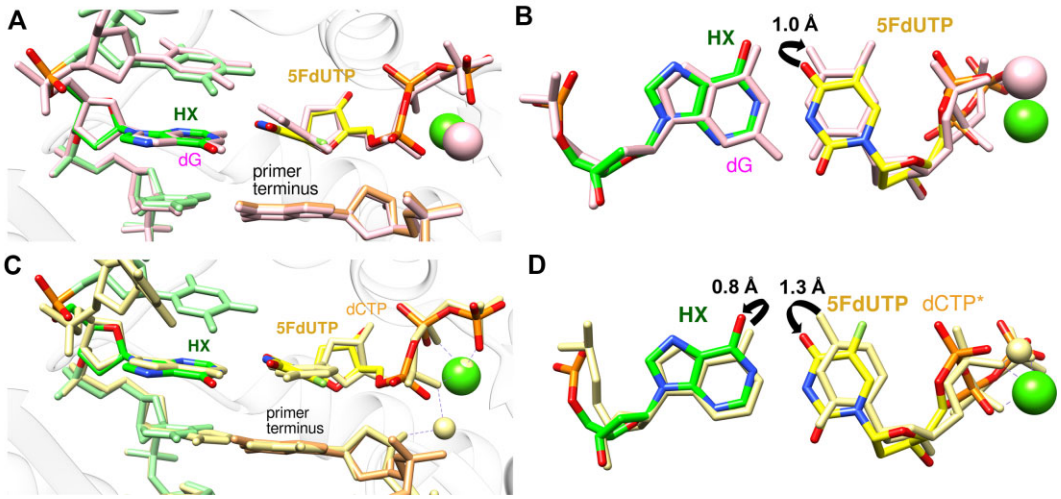

Figure 8. The comparison of structure of polη-HX:5FdUTP with polη-dG:5FdUTP and polη-HX:dCTP* (PDB ID: 6MQ8). (**A**) Close-up view of the overlapped structures of HX:5FdUTP and dG:5FdUTP in the active site of polη. Both base pairs are well ordered and aligned in the active site, yet the position of 5FdUTP in dG:5FdUTP shows significantly greater distortion than in HX:5FdUTP. (**B**) The overlapped structures of the base pairs showed that there was a 1.0 Å difference in the position of 5FdUTP in the two structures due to the greater ring distortion in the base pair of dG:5FdUTP. (**C**) Close-up view of the overlapped structures of HX:5FdUTP and HX:dCTP* in the active site of polη. Both base pairs are well ordered and well aligned in the active site. However, HX:5FdUTP base pair, with just one calcium ion, displays clear ring distortion compared to HX:dCTP*. (**D**) The overlapped structures of the base pairs showed that there was difference in the positions of both HX ring (0.8 Å) and 5FdUTP/dCTP* (1.3 Å) in the two structures.

Incorporation of 5-FU opposite HX leading to increased mutagenicity

When polη-HX:5FdUTP and polη-dG:5FdUTP (pink) structures were superimposed, we were able to gain some insights into the DNA incorporation of 5FdUTP by polη across DNA lesion, which can bring up TLS polymerases. As stated in the previous section, our kinetic studies showed that 5FdUTP incorporation across HX was more efficient than 5FdUTP incorporation across dG (0.37 for HX:5FdUTP versus 0.25 for dG:5FdUTP in terms of $k_{cat}/K_{m,}$ Table 1). When we superimposed the two crystal structures, they overlapped quite well with the RMSD of 0.19 Å over 424 α-carbons along with similar base pairs in the active site of polη (Figure 8A). Though 5FdUTP in the two structures are in different positions (∼1.0 Å), the overall base pairs in the two structures overlapped quite well. Also, the distortion angle in the base pairing is much smaller in HX:5FdUTP than dG:5FdUTP (Figure 8A). Interestingly, the positions of the catalytic metals of Ca^{2+} in the two structures are slightly different with the calcium ion in dG:5FdUTP structure lying in a different position than the canonical metal binding site (Figure 7C), leading to ∼1.5-fold lower reaction efficiency for dG:5FdUTP incorporation compared to HX:5FdUTP (Figure 8B).

Role of DNA lesion, inosine, on the incorporation and bypass of 5FdUTP by polη

To investigate the effect of hypoxanthine lesion in DNA on the incorporation of 5FdUTP, we compared polη-HX:5FdUTP structure with polη-HX:dCTP* (PDB ID: 6MQ8) structure, which is a correct insertion for HX. When the two structures were superimposed, we were able to gain some insights into the DNA incorporation of 5FdUTP across HX, which is an incorrect insertion, by polη. As presented in the earlier section, our kinetic studies showed that 5FdUTP incorporation across HX was approximately 28-fold less efficient than 5FdUTP incorporation across dA (0.37 for HX:5FdUTP versus 10.3 for dA:5FdUTP in terms of $k_{cat}/K_{m,}$ Table 1). When the two crystal structures were superimposed, they overlapped quite well with the RMSD of 0.26 Å over 424 α-carbons (Figure 8C). However, the two base pairs of HX:5FdUTP and HX:dCTP* showed a significant difference in the active site of polη. Approximately 18° distortion of the two rings in the base pair between HX and 5FdUTP is clearly seen in the overlapped structures (Figure 8C), and this distortion caused approximately 0.8 Å difference in the positions of HX and 1.3 Å difference in the positions of 5FdUTP and dCTP* in the two structures (Figure 8D). Also, one of the catalytic metals is missing in the usual position close to Pα of the incoming nucleotide in HX:5FdUTP structure, and this missing catalytic metal combined with less-than-optimal base pair caused the base pair between HX and 5FdUTP to be less efficient than HX:dCTP (Figure 8D). Lastly, the overlapped structures clearly show that the presence of 5-F group (and its interaction with α-phosphate group) on 5FdUTP makes the base pairing interactions between HX and 5FdUTP less optimal compared to the base pairing interactions of HX:dCTP (Figures 6D and 8D). Though the incorporation of 5FdUTP opposite HX is an incorrect insertion, the base pair of HX:5FdUTP in the active site of polη still maintained quite good geometry leading to the increased mutagenicity.

Inosine triphosphatase (ITPase) and DNA polymerase β (polβ) were also upregulated by 5-FU treatment at high concentration

Our qRT-PCR data showed that there are several other genes, in addition to polη, which were upregulated within 72 h of 5-FU treatment in HCT116 cell line. The first notable one is *ITPA* (inosine triphosphatase), which is involved in the clearance of non-canonical triphosphates such as (d)ITP. At 10 μM concentration of 5-FU, *ITPA* was upregulated >2-fold in 72 h (Figure 9A), which is consistent with the previous finding that the overexpression of yeast homolog of ITPase, Ham1p, is closely related to 5-FU resistance (36). Another notable gene that was upregulated was polβ, which is encoded by *POLB* gene, and polβ was upregulated >2-fold upon the

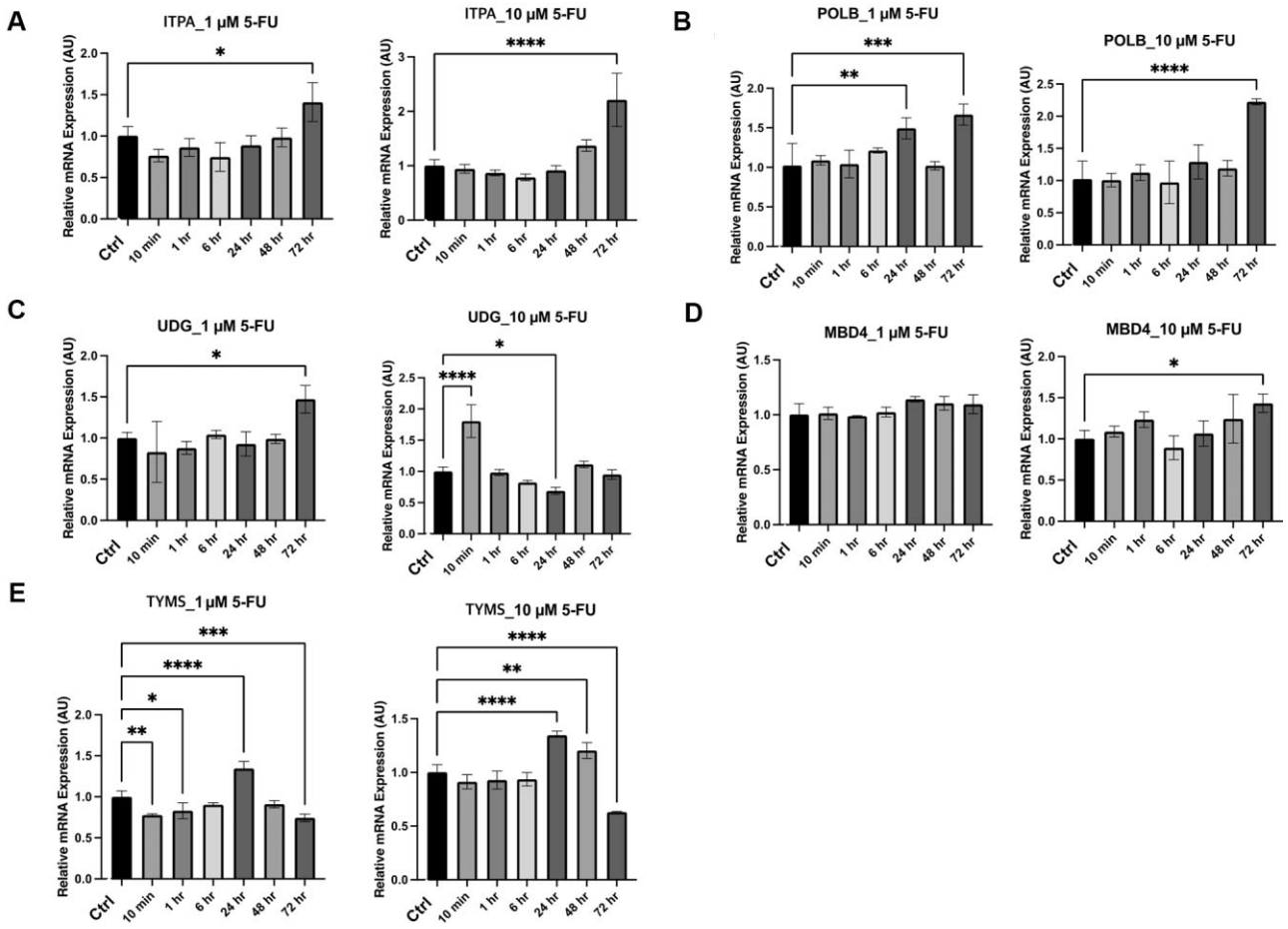

Figure 9. The time-course qRT-PCR experiments for the regulation of gene expression upon 5-FU administration at 1 and 10 μM. The genes tested via qRT-PCR are (**A**) inosine triphosphatase (ITPA), (**B**) DNA polymerase β (polβ), (**C**) uracil DNA glycosylase (UDG), (**D**) methyl-binding domain-4 (MBD4) and (**E**) thymidylate synthase (TYMS).

administration of 5-FU in 72 h (Figure 9B), and polβ was reported to utilize 5FdUTP to incorporate 5-FU into DNA (78). Polβ was shown to be overexpressed in various cancer cells such as ovarian, prostate, melanoma, colon, leukemia and breast cancer cells, and it was also shown that expression levels of polβ in melanoma, colon, and breast cancers were significantly higher compared with the adjacent normal tissues (79,80). It was also shown that polβ can extend a recessed DNA in a concentration as low as 5 nM (51). The upregulation of polβ upon the administration of 5-FU could indicate that polβ, in addition to polη, incorporates 5-FU into DNA in cancer cells, and a crystal structure of polβ incorporating 5-FU was reported (PDB ID: 5WNY) (81). Overall, the detailed roles of the DNA polymerases engaged in the DNA incorporation of 5-FU should further be investigated.

Base excision repair enzymes (UDG/MBD4) and thymidylate synthase (TYMS) were not upregulated upon 5-FU treatment

When 5-FU is incorporated into DNA, it was reported to be removed by base excision repair pathway via uracil DNA glycosylase (UDG) or MBD4 (methyl-CpG binding domain 4) (21,22). However, there has not been any decisive report on how fast 5-FU is incorporated into DNA once it is administered before the DNA repair process is initiated to remove 5-FU from DNA. Our qRT-PCR experiments revealed that there was no significant response in gene expression of UDG (Figure 9C) or MBD4 (Figure 9D) at both 1 and 10 μM concentrations within 72 h after 5-FU treatment. This might indicate that there is a delayed response for the DNA lesion repair process to kick in upon the administration of 5-FU. Another possibility is that DNA repair can be performed for the incorporated 5-FU without any significant changes on the expression of the enzymes in DNA repair at least in CRC. It has yet to be seen how much time DNA repair, especially BER, takes to respond to 5-FU treatment and its incorporation into DNA in cancer cells. By what mechanism BER responds to 5-FU treatment and how cells choose DNA repair over other process such as DNA lesion bypass also remain to be investigated. Another interesting finding was that the main target enzyme for 5-FU, thymidylate synthase (TYMS, Figure 1), was not significantly upregulated upon the administration 5-FU within 72 h either (Figure 9E). This could mean that 5-FU incorporation into DNA via 5FdUTP happens earlier than forming a dead-end complex with TYMS via 5FdUMP.

Discussion

Contributing factors for the mutagenic incorporation of 5FdUTP by polη

Our polη kinetic studies presented here revealed that the catalytic efficiency of 5FdUTP incorporation opposite dA by polη

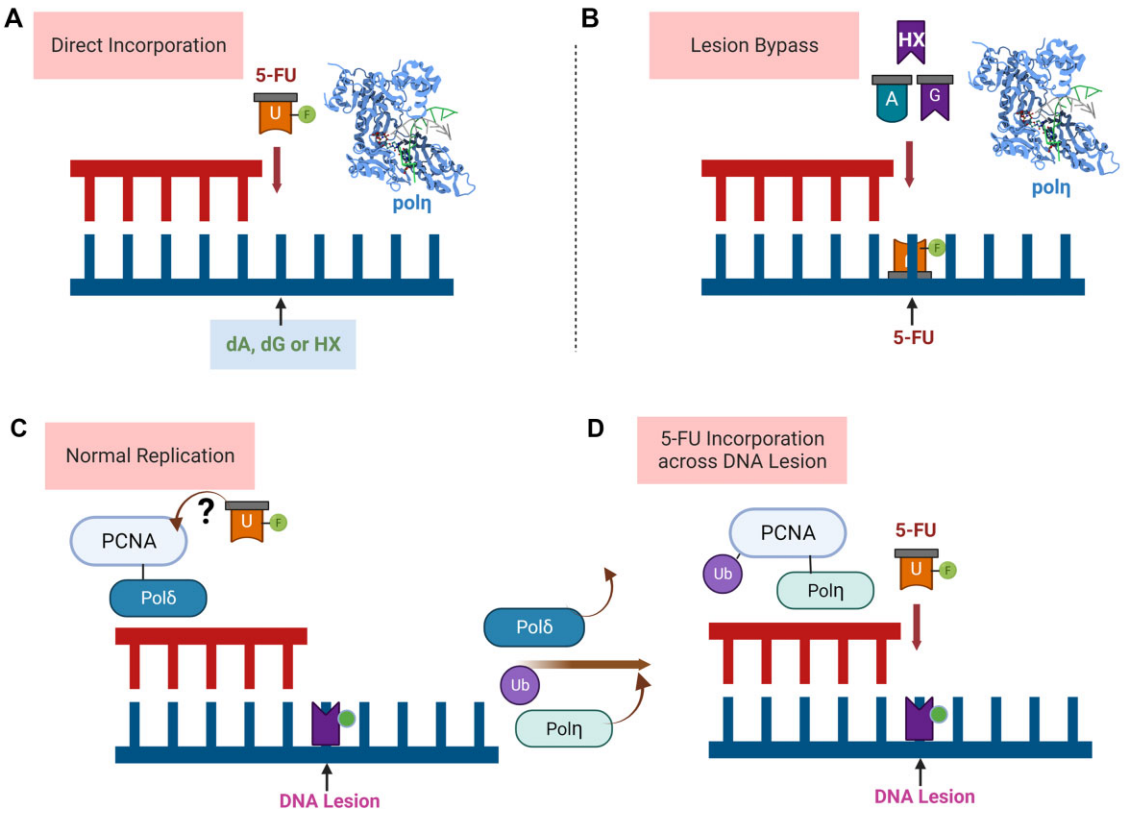

Figure 10. Based on our studies presented here, (**A**) It is clear that polη participated in the direct incorporation of 5-FU across dA, dG and HX. (**B**) It is highly likely that the upregulation of polη indicates that polη is also involved in the lesion bypass once 5-FU is incorporated in DNA. Not just the correct insertion of A, via dATP, but also G, HX and other incorrect/non-canonical bases can be incorporated opposite 5-FU. (**C**) According to the current and previous findings, 5-FU might give a triggering signal to PCNA, which is an assembling clamp for replication, so that a replicative DNA polymerase, such as polδ, is kicked off. This process can also happen when the PCNA complex encounters a DNA lesion such as HX. (**D**) The separation of polδ and the employment of polη happens upon ubiquitination, and the complex of polη and the ubiquitinated PCNA can incorporate 5-FU, via 5FdUTP, across various DNA lesions including HX. Figures prepared using BioRender.

is approximately 41- and 28-fold higher than across dG and HX, respectively. HX is known to act like guanine in DNA, and the combined mutagenicity ratio between across dG/HX and across dA becomes 1:16, which makes the 5-FU incorporation even more mutagenic causing G:C to A:T mutation even after the removal of 5-FU by DNA repair process. This could pose a serious threat to the genome even after 5-FU is successfully removed by DNA repair process. Our kinetic data also showed that polη incorporated dTTP across HX with 0.011 in terms of k_{cat}/K_m and 5FdUTP across HX with 0.037 indicating that 5FdUTP increased the mutagenic incorporation >3-fold, and this result indicates that the presence of a DNA lesion could induce an increased mutagenic incorporation of 5-FU.

The three crystal structures of polη complexed with 5FdUTP across dA, dG, and HX we presented here also give valuable insights into the 5-FU incorporation across both canonical and non-canonical bases. The correct insertion of dA:5FdUTP formed the same base pair as dA:dTTP (Figures 4, 7A and B), while the incorrect insertion of dG:5FdUTP formed a Watson–Crick like base pair via 4-enol tautomer of 5FdUTP (Figure 5). Similarly, a Watson–Crick like base pair was found in HX:5FdUTP (Figure 6), and the incorporation of 5FdUTP across HX was more efficient than dG:5FUTP or HX:dTTP. HX works as guanine in the base pairs, and 5FdUTP incorporation across dG and HX can cause G:C to A:T mutation even after 5-FU is removed from DNA. While the incorporation of 5FdUTP by polη becomes more mutagenic in the presence of inosine, it remains to be seen if any other DNA lesion will affect the same or comparable way as HX does to 5FdUTP incorporation by polη. It suffices to say HX, which works like guanine, can both initiate DNA lesion bypass and increase the replication efficiency along with the mutagenicity. Interestingly both dG:5FdUTP and HX:5FdUTP base pairs are reminiscent of T:G mismatch found in a wide range of DNA polymerases, and T:G mismatch by dGTP insertion opposite dT was reported to happen in various DNA polymerases including polμ (82), polλ (41), polβ (40) and polι (83). The insertion efficiencies of 5FdUTP incorporations by polη across dG and HX were not great enough due to the ring distortions and one catalytic metal found in the two crystal structures (Figure 8A), and further investigations need to be done on whether T:G mismatch can play a role in any way in 5-FU incorporation.

Translesion synthesis and polη might be the first responder upon 5-FU treatment

Our qRT-PCR data revealed that polη, along with polβ, was upregulated significantly upon the administration of 5-FU within 72 h (Figures 2 and 9). In previous studies, polβ was shown to perform like TLS polymerases in fast-growing cells including cancer cells (51), and our qRT-PCR data also shows that polβ is employed in the incorporation of 5-FU. This might also indicate that in cancer environments, where cells grow

fast and the demand for DNA replication is extreme, polη and polβ engage in the same tasks of DNA incorporation and bypass of 5-FU and other lesions to ensure the completion of DNA replication. It was surprising that other TLS enzymes, including polι, polκ or polζ (Supplementary Figure S1A) were not upregulated significantly, except for Rev1 (Supplementary Figure S1B), in response to 5-FU treatment, and this could indicate that polη and Rev1, not other TLS polymerases, are the first to respond to 5-FU treatment for the incorporation of 5-FU into DNA (Figure 2). It was also shown that a replicative DNA polymerase, polδ, was not upregulated in response to 5-FU treatment either, and this might indicate that 5-FU triggers the employment of non-replicative DNA polymerases, including polη or polβ, instead of overexpressing polδ to incorporate 5-FU. To confirm that our findings are not cell line specific, we repeated our qRT-PCR experiments with another colorectal cancer cell line, CaCo2. The upregulation of polη was also observed in CaCo2 cell line (Supplementary Figure S2A), and the gene expression upon 5-FU treatment in CaCo2 cells for other TLS polymerases including poli, polκ, Rev1 and polζ (Supplementary Figure S2B–E) were quite similar. The only difference found was the upregulation of polδ (Supplementary Figure S2F) in CaCo2 cells, and further investigation should be conducted on the role of replicative DNA polymerases including polδ in 5-FU incorporation into DNA. One more thing to note is that the enzymes in base excision repair (BER), UDG and MBD4, were not upregulated either upon 5-FU treatment within 72 hours (Figures 2 and 9), and this indicates that BER kicks in later than 5-FU incorporation or the lesion bypass of 5-FU at least in HCT116 colorectal cancer cell line. The gene expression results for the enzymes involved in DNA repair and nucleotide biosynthesis, ITPA, polβ, UDG, MBD4, and TYMS (Supplementary Figure S3A–E), in CaCo2 cells were consistent with HCT116 cells. To our knowledge, there is no definite evidence on which one, between DNA repair and DNA lesion bypass, kicks in first in response of 5-FU, and our studies here might suggest that DNA bypass enzyme, polη, responds first to 5-FU treatment in incorporating and bypassing 5-FU in DNA.

Proposed mechanism of the role of polη and TLS for DNA incorporation and lesion bypass of 5-FU

Our data presented here clearly confirmed that polη incorporates 5-FU into DNA across dA, dG, and HX (Figure 10A). Though it remains to be seen if polη can incorporate 5-FU across other DNA lesions, our data presented here revealed that 5-FU incorporation can happen across both canonical and non-canonical bases. Once 5-FU is incorporated into DNA, that strand can be used as a template for the next round of replication. Then, polη and TLS will perform DNA lesion bypass across 5-FU by incorporating canonical and non-canonical nucleotides (Figure 10B). It is not clear if this lesion bypass happens within 72 hours upon the administration of 5-FU (Figure 2C), and further investigation on lesion bypass across 5-FU by polη is underway in our lab as well. One important question remaining is how TLS machinery, which consists of proliferating cell nuclear antigen (PCNA) along with DNA polymerases and other components, is triggered upon 5-FU treatment for polη to incorporate 5-FU into DNA. This process requires the detachment of replicative polymerase including polδ, the ubiquitination of PCNA, and the employment of polη (Figure 10C). Usually, DNA lesions, including HX, initiate this process of polymerase switch (84–87), and our experimental data suggest that 5-FU might be another trigger for PCNA to kick off polδ and bring in polη. Based on our observation that polη was highly upregulated in 72 h upon 5-FU treatment in HCT116 cell line, there might be a specific signaling function of 5-FU that triggers the employment of polη to incorporate and/or to bypass 5-FU. Theoretically, once 5-FU is incorporated in DNA, it can be used as a template without any significant delay, and polη, which is attached to the ubiquitylated PCNA, can incorporate 5-FU across DNA lesions (Figure 10D). It is highly likely that polη incorporates 5FdUTP across a wide range of DNA lesions, especially purine-base containing lesions, in fast growing cells like cancer cells, where the replication demand is heavy. Also, the involvement of polη and TLS in the incorporation and bypass of 5-FU might have a significant impact on the mechanism of drug action and drug resistance of 5-FU, and further research will give us more detailed answers on the relationship between TLS/polη and the drug action/resistance caused by 5-FU and other anticancer drugs. Also, it would be worthwhile to see if translesion synthesis and polη have similar roles on the direct incorporation and bypass of other nucleotide analog drugs such as gemcitabine or 6-thiopurine.

In conclusion, our cell biological, structural, and biochemical studies presented here using HCT116 cells and polη provide novel insights into the mutagenic potential of one of the major anticancer agents, 5-FU. In response to 5-FU treatment in HCT116 cell line, polη was upregulated to insert 5-FU across canonical and non-canonical bases with increased mutagenicity that can cause G:C to A:T mutation. The reaction efficiency was higher for dG:5FdUTP and HX:5FdUTP than dG:dTTP and HX:dTTP resulting in the increased mutagenicity in 5FdUTP incorporation. The crystal structures of polη revealed that dG and HX formed Watson–Crick like base pairs with 4-enol tautomer of 5-FU. We have observed that polη, along with polβ and Rev1, was upregulated upon 5-FU treatment, and 5-FU might work as a trigger that causes the dissociation of polδ from PCNA and the association of polη on PCNA for the incorporation of 5-FU by polη. These findings might have significant insight in overcoming the drug resistance of 5-FU that is caused by DNA lesion bypass of 5-FU.

Data availability

The atomic coordinates of Polη-DNA complexed with 5FdUTP have been deposited in the Protein Data Bank with the following accession codes: Polη-dA:5FdUTP (PDB Code: 8GKR), Polη-dG:5FdUTP (PDB Code: 8GML), and Polη-HX:5FdUTP (PDB Code: 8SKI).

Supplementary data

Supplementary Data are available at NAR Online.

Acknowledgements

The authors are grateful to Dr SooWan Lee (School of Pharmacy, University of Connecticut) for the help on HCT116 cell culture and qRT-PCR experiment. This research was supported by the School of Pharmacy at the University of Connecticut.

Funding

National Institute of General Medical Sciences [P41GM111244]; U.S. Department of Energy (DOE) Office of Biological and Environmental Research [KP1605010]; U.S. Department of Energy (DOE) Office of Basic Energy Sciences (contract number: DE-SC0012704) [KC0401040]. Funding for open access charge: Start-up fund from the University of Connecticut.

Conflict of interest statement

The authors declare no conflict of interest.

References

1. Siegel,R.L., Miller,K.D., Goding Sauer,A., Fedewa,S.A., Butterly,L.F., Anderson,J.C., Cercek,A., Smith,R.A. and Jemal,A. (2020) Colorectal cancer statistics, 2020. *CA Cancer J. Clin.*, **70**, 145–164.
2. Bray,F., Ferlay,J., Soerjomataram,I., Siegel,R.L., Torre,L.A. and Jemal,A. (2018) Global cancer statistics 2018: GLOBOCAN estimates of incidence and mortality worldwide for 36 cancers in 185 countries. *CA Cancer J. Clin.*, **68**, 394–424.
3. Hurwitz,H.I., Tan,B.R., Reeves,J.A., Xiong,H., Somer,B., Lenz,H.J., Hochster,H.S., Scappaticci,F., Palma,J.F., Price,R., *et al.* (2019) Phase II Randomized Trial of Sequential or Concurrent FOLFOXIRI-Bevacizumab Versus FOLFOX-Bevacizumab for Metastatic Colorectal Cancer (STEAM). *Oncologist*, **24**, 921–932.
4. Tsuji,S., Midorikawa,Y., Takahashi,T., Yagi,K., Takayama,T., Yoshida,K., Sugiyama,Y. and Aburatani,H. (2012) Potential responders to FOLFOX therapy for colorectal cancer by Random Forests analysis. *Br. J. Cancer*, **106**, 126–132.
5. Nagourney,R.A., Evans,S., Tran,P.H., Nagourney,A.J. and Sugarbaker,P.H. (2021) Colorectal cancer cells from patients treated with FOLFOX or CAPOX are resistant to oxaliplatin. *Eur. J. Surg. Oncol.*, **47**, 738–742.
6. Miura,K., Kinouchi,M., Ishida,K., Fujibuchi,W., Naitoh,T., Ogawa,H., Ando,T., Yazaki,N., Watanabe,K., Haneda,S., *et al.* (2010) 5-fu metabolism in cancer and orally-administrable 5-fu drugs. *Cancers (Basel)*, **2**, 1717–1730.
7. Longley,D.B., Harkin,D.P. and Johnston,P.G. (2003) 5-fluorouracil: mechanisms of action and clinical strategies. *Nat. Rev. Cancer*, **3**, 330–338.
8. Danenberg,P.V., Heidelberger,C., Mulkins,M.A. and Peterson,A.R. (1981) The incorporation of 5-fluoro-2'-deoxyuridine into DNA of mammalian tumor cells. *Biochem. Biophys. Res. Commun.*, **102**, 654–658.
9. Cheng,Y.C. and Nakayama,K. (1983) Effects of 5-fluoro-2'-deoxyuridine on DNA metabolism in HeLa cells. *Mol. Pharmacol.*, **23**, 171–174.
10. Ingraham,H.A., Tseng,B.Y. and Goulian,M. (1982) Nucleotide levels and incorporation of 5-fluorouracil and uracil into DNA of cells treated with 5-fluorodeoxyuridine. *Mol. Pharmacol.*, **21**, 211–216.
11. Lonn,U. and Lonn,S. (1986) DNA lesions in human neoplastic cells and cytotoxicity of 5-fluoropyrimidines. *Cancer Res.*, **46**, 3866–3870.
12. Major,P.P., Egan,E., Herrick,D. and Kufe,D.W. (1982) 5-Fluorouracil incorporation in DNA of human breast carcinoma cells. *Cancer Res.*, **42**, 3005–3009.
13. Parker,W.B., Kennedy,K.A. and Klubes,P. (1987) Dissociation of 5-fluorouracil-induced DNA fragmentation from either its incorporation into DNA or its cytotoxicity in murine T-lymphoma (S-49) cells. *Cancer Res.*, **47**, 979–982.
14. Peters,G.J., Noordhuis,P., Komissarov,A., Holwerda,U., Kok,M., Van Laar,J.A., Van der Wilt,C.L., Van Groeningen,V. and Pinedo,H.M. (1995) Quantification of 5-fluorouracil incorporation into RNA of human and murine tumors as measured with a sensitive gas chromatography-mass spectrometry assay. *Anal. Biochem.*, **231**, 157–163.
15. Noordhuis,P., Holwerda,U., Van der Wilt,C.L., Van Groeningen,C.J., Smid,K., Meijer,S., Pinedo,H.M. and Peters,G.J. (2004) 5-Fluorouracil incorporation into RNA and DNA in relation to thymidylate synthase inhibition of human colorectal cancers. *Ann. Oncol.*, **15**, 1025–1032.
16. Peters,H., Eisenberg,R., Daig,U., Liefeldt,L., Westenfeld,R., Gaedeke,J., Kramer,S. and Neumayer,H.H. (2004) Platelet inhibition limits TGF-beta overexpression and matrix expansion after induction of anti-thy1 glomerulonephritis. *Kidney Int.*, **65**, 2238–2248.
17. Xie,K., Doles,J., Hemann,M.T. and Walker,G.C. (2010) Error-prone translesion synthesis mediates acquired chemoresistance. *Proc. Natl. Acad. Sci. USA*, **107**, 20792–20797.
18. Siddik,Z.H. (2003) Cisplatin: mode of cytotoxic action and molecular basis of resistance. *Oncogene*, **22**, 7265–7279.
19. Tomicic,M.T., Aasland,D., Naumann,S.C., Meise,R., Barckhausen,C., Kaina,B. and Christmann,M. (2014) Translesion polymerase eta is upregulated by cancer therapeutics and confers anticancer drug resistance. *Cancer Res.*, **74**, 5585–5596.
20. Sun,X., Hou,W., Liu,X., Chai,J., Guo,H. and Yu,J. (2020) Targeting REV7 effectively reverses 5-FU and oxaliplatin resistance in colorectal cancer. *Cancer Cell Int.*, **20**, 580.
21. Ingraham,H.A., Tseng,B.Y. and Goulian,M. (1980) Mechanism for exclusion of 5-fluorouracil from DNA. *Cancer Res.*, **40**, 998–1001.
22. Fischer,F., Baerenfaller,K. and Jiricny,J. (2007) 5-Fluorouracil is efficiently removed from DNA by the base excision and mismatch repair systems. *Gastroenterology*, **133**, 1858–1868.
23. Pettersen,H.S., Visnes,T., Vagbo,C.B., Svaasand,E.K., Doseth,B., Slupphaug,G., Kavli,B. and Krokan,H.E. (2011) UNG-initiated base excision repair is the major repair route for 5-fluorouracil in DNA, but 5-fluorouracil cytotoxicity depends mainly on RNA incorporation. *Nucleic Acids Res.*, **39**, 8430–8444.
24. Kunz,C., Focke,F., Saito,Y., Schuermann,D., Lettieri,T., Selfridge,J. and Schar,P. (2009) Base excision by thymine DNA glycosylase mediates DNA-directed cytotoxicity of 5-fluorouracil. *PLoS Biol.*, **7**, e91.
25. Bader,S., Walker,M. and Harrison,D. (2000) Most microsatellite unstable sporadic colorectal carcinomas carry MBD4 mutations. *Br. J. Cancer*, **83**, 1646–1649.
26. Riccio,A., Aaltonen,L.A., Godwin,A.K., Loukola,A., Percesepe,A., Salovaara,R., Masciullo,V., Genuardi,M., Paravatou-Petsotas,M., Bassi,D.E., *et al.* (1999) The DNA repair gene MBD4 (MED1) is mutated in human carcinomas with microsatellite instability. *Nat. Genet.*, **23**, 266–268.
27. Caulfield,J.L., Wishnok,J.S. and Tannenbaum,S.R. (1998) Nitric oxide-induced deamination of cytosine and guanine in deoxynucleosides and oligonucleotides. *J. Biol. Chem.*, **273**, 12689–12695.
28. Wink,D.A., Kasprzak,K.S., Maragos,C.M., Elespuru,R.K., Misra,M., Dunams,T.M., Cebula,T.A., Koch,W.H., Andrews,A.W., Allen,J.S., *et al.* (1991) DNA deaminating ability and genotoxicity of nitric oxide and its progenitors. *Science*, **254**, 1001–1003.
29. Jung,H., Hawkins,M. and Lee,S. (2020) Structural insights into the bypass of the major deaminated purines by translesion synthesis DNA polymerase. *Biochem. J.*, **477**, 4797–4810.
30. Averill,J.R. and Jung,H. (2023) Mutagenic incorporation of inosine into DNA via T:i mismatch formation by human DNA polymerase eta (poleta). *Biochem. J.*, **480**, 649–664.
31. DeVito,S., Woodrick,J., Song,L. and Roy,R. (2017) Mutagenic potential of hypoxanthine in live human cells. *Mutat. Res.*, **803-805**, 9–16.
32. Fraser,J.H., Meyers,H., Henderson,J.F., Brox,L.W. and McCoy,E.E. (1975) Individual variation in inosine triphosphate accumulation in human erythrocytes. *Clin. Biochem.*, **8**, 353–364.
33. Kevelam,S.H., Bierau,J., Salvarinova,R., Agrawal,S., Honzik,T., Visser,D., Weiss,M.M., Salomons,G.S., Abbink,T.E., Waisfisz,Q.,

et al. (2015) Recessive ITPA mutations cause an early infantile encephalopathy. *Ann. Neurol.*, **78**, 649–658.
34. Handley,M.T., Reddy,K., Wills,J., Rosser,E., Kamath,A., Halachev,M., Falkous,G., Williams,D., Cox,P., Meynert,A., *et al.* (2019) ITPase deficiency causes a Martsolf-like syndrome with a lethal infantile dilated cardiomyopathy. *PLoS Genet.*, **15**, e1007605.
35. Koga,Y., Tsuchimoto,D., Hayashi,Y., Abolhassani,N., Yoneshima,Y., Sakumi,K., Nakanishi,H., Toyokuni,S. and Nakabeppu,Y. (2020) Neural stem cell-specific ITPA deficiency causes neural depolarization and epilepsy. *JCI Insight*, **5**, e140229.
36. Carlsson,M., Gustavsson,M., Hu,G.Z., Muren,E. and Ronne,H. (2013) A Ham1p-dependent mechanism and modulation of the pyrimidine biosynthetic pathway can both confer resistance to 5-fluorouracil in yeast. *PLoS One*, **8**, e52094.
37. Takayama,S., Fujii,M., Kurosawa,A., Adachi,N. and Ayusawa,D. (2007) Overexpression of HAM1 gene detoxifies 5-bromodeoxyuridine in the yeast Saccharomyces cerevisiae. *Curr. Genet.*, **52**, 203–211.
38. Arana,M.E. and Kunkel,T.A. (2010) Mutator phenotypes due to DNA replication infidelity. *Semin. Cancer Biol.*, **20**, 304–311.
39. Cooper,D.N., Mort,M., Stenson,P.D., Ball,E.V. and Chuzhanova,N.A. (2010) Methylation-mediated deamination of 5-methylcytosine appears to give rise to mutations causing human inherited disease in CpNpG trinucleotides, as well as in CpG dinucleotides. *Hum. Genomics*, **4**, 406–410.
40. Kunkel,T.A. (1985) The mutational specificity of DNA polymerases-alpha and -gamma during in vitro DNA synthesis. *J. Biol. Chem.*, **260**, 12866–12874.
41. Bebenek,K., Pedersen,L.C. and Kunkel,T.A. (2011) Replication infidelity via a mismatch with Watson-Crick geometry. *Proc. Natl. Acad. Sci. USA*, **108**, 1862–1867.
42. Cortellino,S., Turner,D., Masciullo,V., Schepis,F., Albino,D., Daniel,R., Skalka,A.M., Meropol,N.J., Alberti,C., Larue,L., *et al.* (2003) The base excision repair enzyme MED1 mediates DNA damage response to antitumor drugs and is associated with mismatch repair system integrity. *Proc. Natl. Acad. Sci. USA*, **100**, 15071–15076.
43. Ouzon-Shubeita,H., Jung,H., Lee,M.H., Koag,M.C. and Lee,S. (2020) Catalytic mechanism of the mismatch-specific DNA glycosylase methyl-CpG-binding domain 4. *Biochem. J.*, **477**, 1601–1612.
44. Knobel,P.A. and Marti,T.M. (2011) Translesion DNA synthesis in the context of cancer research. *Cancer Cell Int.*, **11**, 39.
45. Kannouche,P.L. and Lehmann,A.R. (2004) Ubiquitination of PCNA and the polymerase switch in human cells. *Cell Cycle*, **3**, 1011–1013.
46. Yasui,M., Suzuki,N., Miller,H., Matsuda,T., Matsui,S. and Shibutani,S. (2004) Translesion synthesis past 2'-deoxyxanthosine, a nitric oxide-derived DNA adduct, by mammalian DNA polymerases. *J. Mol. Biol.*, **344**, 665–674.
47. Sale,J.E., Lehmann,A.R. and Woodgate,R. (2012) Y-family DNA polymerases and their role in tolerance of cellular DNA damage. *Nat. Rev. Mol. Cell Biol.*, **13**, 141–152.
48. Vaisman,A., Ling,H., Woodgate,R. and Yang,W. (2005) Fidelity of Dpo4: effect of metal ions, nucleotide selection and pyrophosphorolysis. *EMBO J.*, **24**, 2957–2967.
49. Jung,H. and Lee,S. (2020) Promutagenic bypass of 7,8-dihydro-8-oxoadenine by translesion synthesis DNA polymerase Dpo4. *Biochem. J.*, **477**, 2859–2871.
50. Jung,H. and Lee,S. (2021) Insights into the mismatch discrimination mechanism of Y-family DNA polymerase Dpo4. *Biochem. J.*, **478**, 1769–1781.
51. Koag,M.C., Jung,H. and Lee,S. (2019) Mutagenic Replication of the Major Oxidative Adenine Lesion 7,8-Dihydro-8-oxoadenine by Human DNA Polymerases. *J. Am. Chem. Soc.*, **141**, 4584–4596.
52. Koag,M.C., Jung,H. and Lee,S. (2020) Mutagenesis mechanism of the major oxidative adenine lesion 7,8-dihydro-8-oxoadenine. *Nucleic Acids Res.*, **48**, 5119–5134.
53. Zhao,Y., Biertumpfel,C., Gregory,M.T., Hua,Y.J., Hanaoka,F. and Yang,W. (2012) Structural basis of human DNA polymerase eta-mediated chemoresistance to cisplatin. *Proc. Natl. Acad. Sci. USA*, **109**, 7269–7274.
54. Biertumpfel,C., Zhao,Y., Kondo,Y., Ramon-Maiques,S., Gregory,M., Lee,J.Y., Masutani,C., Lehmann,A.R., Hanaoka,F. and Yang,W. (2010) Structure and mechanism of human DNA polymerase eta. *Nature*, **465**, 1044–1048.
55. Patra,A., Zhang,Q., Guengerich,F.P. and Egli,M. (2016) Mechanisms of Insertion of dCTP and dTTP Opposite the DNA Lesion O6-Methyl-2'-deoxyguanosine by Human DNA Polymerase eta. *J. Biol. Chem.*, **291**, 24304–24313.
56. Koag,M.C., Jung,H., Kou,Y. and Lee,S. (2019) Bypass of the major alkylative DNA lesion by human DNA polymerase eta. *Molecules*, **24**, 3928.
57. Jung,H., Rayala,N.K. and Lee,S. (2022) Effects of N7-alkylguanine conformation and metal cofactors on the translesion synthesis by human DNA polymerase η. *Chem. Res. Toxicol.*, **35**, 512–521.
58. Jung,H., Rayala,N.K. and Lee,S. (2020) Translesion synthesis of the major nitrogen mustard-induced DNA lesion by human DNA polymerase eta. *Biochem. J.*, **477**, 4543–4558.
59. Jung,H. (2022) Contributing factors for mutagenic DNA lesion bypass by DNA polymerase eta (polη). *DNA*, **2**, 205–220.
60. Jung,H. and Lee,S. (2020) Promutagenic bypass of 7,8-dihydro-8-oxoadenine by translesion synthesis DNA polymerase Dpo4. *Biochem J.*, **477**, 2859–2871.
61. Kabsch,W. (2010) Xds. *Acta. Crystallogr. D Biol. Crystallogr.*, **66**, 125–132.
62. Kabsch,W. (2010) Integration, scaling, space-group assignment and post-refinement. *Acta. Crystallogr. D Biol. Crystallogr.*, **66**, 133–144.
63. Karplus,P.A. and Diederichs,K. (2012) Linking crystallographic model and data quality. *Science*, **336**, 1030–1033.
64. Evans,P.R. and Murshudov,G.N. (2013) How good are my data and what is the resolution?*Acta. Crystallogr. D Biol. Crystallogr.*, **69**, 1204–1214.
65. Vagin,A. and Teplyakov,A. (2010) Molecular replacement with MOLREP. *Acta. Crystallogr. D Biol. Crystallogr.*, **66**, 22–25.
66. Emsley,P. and Cowtan,K. (2004) Coot: model-building tools for molecular graphics. *Acta. Crystallogr. D Biol. Crystallogr.*, **60**, 2126–2132.
67. Liebschner,D., Afonine,P.V., Baker,M.L., Bunkóczi,G., Chen,V.B., Croll,T.I., Hintze,B., Hung,L.W., Jain,S., McCoy,A.J., *et al.* (2019) Macromolecular structure determination using X-rays, neutrons and electrons: recent developments in Phenix. *Acta Crystallogr D Struct. Biol.*, **75**, 861–877.
68. Chen,V.B., Arendall,W.B., Headd,J.J., Keedy,D.A., Immormino,R.M., Kapral,G.J., Murray,L.W., Richardson,J.S. and Richardson,D.C. (2010) MolProbity: all-atom structure validation for macromolecular crystallography. *Acta. Crystallogr. D Biol. Crystallogr.*, **66**, 12–21.
69. Pettersen,E.F., Goddard,T.D., Huang,C.C., Couch,G.S., Greenblatt,D.M., Meng,E.C. and Ferrin,T.E. (2004) UCSF Chimera–a visualization system for exploratory research and analysis. *J. Comput. Chem.*, **25**, 1605–1612.
70. Yasui,M., Suenaga,E., Koyama,N., Masutani,C., Hanaoka,F., Gruz,P., Shibutani,S., Nohmi,T., Hayashi,M. and Honma,M. (2008) Miscoding properties of 2'-deoxyinosine, a nitric oxide-derived DNA Adduct, during translesion synthesis catalyzed by human DNA polymerases. *J. Mol. Biol.*, **377**, 1015–1023.
71. Bickley,J., Short,J.K., McDowell,D.G. and Parkes,H.C. (1996) Polymerase chain reaction (PCR) detection of Listeria monocytogenes in diluted milk and reversal of PCR inhibition caused by calcium ions. *Lett. Appl. Microbiol.*, **22**, 153–158.
72. Opel,K.L., Chung,D. and McCord,B.R. (2010) A study of PCR inhibition mechanisms using real time PCR. *J. Forensic Sci.*, **55**, 25–33.

73. Nakamura,T., Zhao,Y., Yamagata,Y., Hua,Y.J. and Yang,W. (2012) Watching DNA polymerase eta make a phosphodiester bond. *Nature*, **487**, 196–201.
74. Su,Y., Patra,A., Harp,J.M., Egli,M. and Guengerich,F.P. (2015) Roles of Residues Arg-61 and Gln-38 of Human DNA Polymerase eta in Bypass of Deoxyguanosine and 7,8-Dihydro-8-oxo-2'-deoxyguanosine. *J. Biol. Chem.*, **290**, 15921–15933.
75. Parker,J.B. and Stivers,J.T. (2011) Dynamics of uracil and 5-fluorouracil in DNA. *Biochemistry*, **50**, 612–617.
76. Sowers,L.C., Eritja,R., Kaplan,B., Goodman,M.F. and Fazakerly,G.V. (1988) Equilibrium between a wobble and ionized base pair formed between fluorouracil and guanine in DNA as studied by proton and fluorine NMR. *J. Biol. Chem.*, **263**, 14794–14801.
77. Yu,H., Eritja,R., Bloom,L.B. and Goodman,M.F. (1993) Ionization of bromouracil and fluorouracil stimulates base mispairing frequencies with guanine. *J. Biol. Chem.*, **268**, 15935–15943.
78. Tanaka,M., Yoshida,S., Saneyoshi,M. and Yamaguchi,T. (1981) Utilization of 5-fluoro-2'-deoxyuridine triphosphate and 5-fluoro-2'-deoxycytidine triphosphate in DNA synthesis by DNA polymerases alpha and beta from calf thymus. *Cancer Res.*, **41**, 4132–4135.
79. Srivastava,D.K., Husain,I., Arteaga,C.L. and Wilson,S.H. (1999) DNA polymerase beta expression differences in selected human tumors and cell lines. *Carcinogenesis*, **20**, 1049–1054.
80. Servant,L., Cazaux,C., Bieth,A., Iwai,S., Hanaoka,F. and Hoffmann,J.S. (2002) A role for DNA polymerase beta in mutagenic UV lesion bypass. *J. Biol. Chem.*, **277**, 50046–50053.
81. Schaich,M.A., Smith,M.R., Cloud,A.S., Holloran,S.M. and Freudenthal,B.D. (2017) Structures of a DNA Polymerase Inserting Therapeutic Nucleotide Analogues. *Chem. Res. Toxicol.*, **30**, 1993–2001.
82. Caglayan,M. and Wilson,S.H. (2018) Pol mu dGTP mismatch insertion opposite T coupled with ligation reveals promutagenic DNA repair intermediate. *Nat. Commun.*, **9**, 4213.
83. Jain,R., Nair,D.T., Johnson,R.E., Prakash,L., Prakash,S. and Aggarwal,A.K. (2009) Replication across template T/U by human DNA polymerase-iota. *Structure*, **17**, 974–980.
84. Hoege,C., Pfander,B., Moldovan,G.L., Pyrowolakis,G. and Jentsch,S. (2002) RAD6-dependent DNA repair is linked to modification of PCNA by ubiquitin and SUMO. *Nature*, **419**, 135–141.
85. Moldovan,G.L., Pfander,B. and Jentsch,S. (2007) PCNA, the maestro of the replication fork. *Cell*, **129**, 665–679.
86. Haracska,L., Yu,S.L., Johnson,R.E., Prakash,L. and Prakash,S. (2000) Efficient and accurate replication in the presence of 7,8-dihydro-8-oxoguanine by DNA polymerase eta. *Nat. Genet.*, **25**, 458–461.
87. Bergink,S. and Jentsch,S. (2009) Principles of ubiquitin and SUMO modifications in DNA repair. *Nature*, **458**, 461–467.

Received: September 10, 2023. **Revised:** January 12, 2024. **Editorial Decision:** January 30, 2024. **Accepted:** February 1, 2024